



**JIMMA UNIVERSITY**  
**SCHOOL OF GRADUATE STUDIES**  
**JIMMA INSTITUTE OF TECHNOLOGY**  
**FACULTY OF MECHANICAL ENGINEERING**  
**THERMAL SYSTEM ENGINEERING STREAM**

**PERFORMANCE ANALYSIS AND SIMULATION OF SAVONIUS WIND  
TURBINE FOR SMALL-SCALE WATER PUMPING SYSTEM**

BY: Abeba Negewo

A thesis submitted to the School of Graduate Studies of Jimma Institute of Technology, Jimma University in Partial fulfillment of the requirements for the award of Masters of Science in Thermal System Engineering

December 2022

JIMMA, ETHIOPIA

Performance Analysis and Simulation of Savonius Wind Turbine for Small-Scale Water Pumping System

JIMMA UNIVERSITY  
SCHOOL OF GRADUATE STUDIES  
JIMMA INSTITUTE OF TECHNOLOGY  
FACULTY OF MECHANICAL ENGINEERING

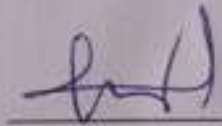
Performance Analysis and Simulation of Savonius Wind Turbine for Small-Scale Water Pumping System

By: Abeba Negewo

Examining Committee:

Main Advisor

Mr. Balewgize A. Zeru (Asst. Prof.)



Signature

21/12/2022

Date

Co-Advisor

Mr. Demeke Girma (MSc)



Signature

21/12/2022

Date

External Examiner Dr.

Solomon T/Mariam



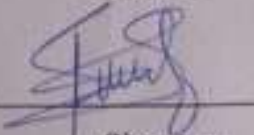
Signature

17/12/2022

Date

Internal Examiner

Mr. Fikru Gebre



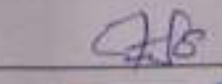
Signature

19/12/2022

Date

Chairman

Mr. Ali Seid



Signature

21/12/2022

Date



Ali Seid  
Thermal System Engineering  
Faculty of Mechanical Engineering

Performance Analysis and Simulation of Savonius Wind Turbine for Small-Scale Water Pumping System

DECLARATION

This is to certify that the thesis entitled, **Performance Analysis and Simulation of Savonius Wind Turbine for Small-Scale Water Pumping System** is my original work, under the Faculty of Mechanical Engineering, Thermal Systems Engineering stream at Jimma Institute of Technology and has not been presented for a degree in any other university and all sources used for the thesis have been duly acknowledged and a list of reference is given.

Abeba Negewo



Signature

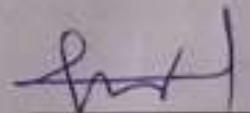
15/12/2022

Date

This thesis/research had been submitted to Jimma University, Faculty of Mechanical Engineering with our approval.

Balewgize A. Zeru (Asst. Prof.)

Main Advisor



Signature

21/12/2022

Date

Mr. Demeke Girma (MSc)

Co-Advisor



Signature

21/12/2022

Date

## ABSTRACT

*Water is the most important source of life, and it is presently accessed through pumps. Centrifugal and positive displacement pumps are two types of pumps, with electrical, diesel, and renewable energy sources (Solar and Wind energies) as inputs. To solve environmental issues, wind energy has emerged as a new energy option. Wind energy is converted to the required energy using turbines. Based on the rotation axis, they are divided into two categories: horizontal and vertical. The Savonius wind rotor is a vertical axis wind turbine (VAWT) with a simple structure and a low operating speed, making it ideal for places with low average wind speeds. However, its application areas are limited due to its low performance. According to studies, the shape and number of blades, rotor stage, shaft influence, overlap ratio, endplate, blade angle of twist, aspect ratio, and fin addition all have a significant impact on S-VAWT performance.*

*The purpose of this study is to use CFD methods to improve the performance of the S-VAWT for the water pumping system in the Dodota area by modifying aspect ratios and adding fins to the blade, and to compare the results to previous literature. The power delivered by the rotor is around 12.8 W while the power available in the wind is 40 W. From the wind power, the size of the rotor is calculated to pump the water needed. The rotor contains four turbine blades with a rotor diameter of 3 m, an endplate diameter of 3.3 m, a rotor height of 2.4 m, and an aspect ratio of 0.8. SOLIDWORK 2018 was used to create the 3D model of the Savonius rotor, and ANSYS 19.2 was utilized to simulate it. The study was carried out throughout the dry season using the National Metrology Agency of Ethiopia wind speed data, with an average value of 2.15 m/s. The fin is used to direct the wind flow by filling the space in the blades. The results showed that when two fins are added, the pressure distributions and velocity distributions are higher than when only one fin is used or when without a fin is used. With the addition of two blades, the power coefficient,  $C_p$  in this study increases by an average of 0.256. This result is higher compared to previously done by Ridwan et al, 2019 which was 0.241.*

## ACKNOWLEDGMENT

The completion of this study taught me far more than I could have expected. It gives me great pleasure to offer my sincere gratitude to a variety of persons who have helped me with ideas and support in various ways. Mr. Balewgize A. Zeru (Asst. Prof.) and Mr. Demeke Girma (MSc) deserve a special thank you for your help, advice, and patience during the thesis work. Also, I want to express my gratitude to Gezahegn L., Network Administrator, for his willingness to assist me with computer access and for appreciating me in each way. It is also my pleasure to express my heartfelt gratitude to Mr. Abraha K., Mr. Leta Y., Mr. Eshetu T., and Mr. Yohannis A. staff member of Jimma University's Faculty of Mechanical Engineering for welcoming me with open arms and presenting me with the ANSYS Manual. Finally, I'd want to thank Mr. Ali Seid, Chairman of Thermal Systems Engineering, and everyone else who assisted me in completing the research. Above all, I am grateful to the Most Gracious, the all-powerful God.

## Table of Contents

DECLARATION .....	ii
ABSTRACT .....	iii
ACKNOWLEDGMENT.....	iv
LIST OF FIGURES .....	viii
LIST OF TABLES .....	x
NOMENCLATURE .....	xi
CHAPTER ONE .....	1
INTRODUCTION .....	1
1.1 Background .....	1
1.2 Statement of the Problem .....	9
1.3 Objectives.....	9
1.3.1 General Objective .....	9
1.3.2 Specific Objectives .....	9
1.4 Justification of the study .....	10
1.5 Scope of the study .....	10
CHAPTER TWO .....	11
LITERATURE REVIEW .....	11
2.1 Wind energy .....	11
2.2 Factors affecting the performance of S-VAWTs (Akwa, Vielmo, and Petry, 2012).....	14
2.3 Improvements made .....	21
2.4 Literature Conclusion and Research Gap.....	21
CHAPTER THREE .....	22
DESIGN AND METHODOLOGY .....	22
3.1 Study Area.....	22

Performance Analysis and Simulation of Savonius Wind Turbine for Small-Scale Water Pumping System

---

3.2 Research Strategies .....	22
3.2.1 Research strategy .....	22
3.2.2 Sources of information.....	23
3.2.3 Working Principles .....	23
3.3 Wind data .....	25
3.4 Aspect Ratio .....	29
3.5 Diameter of the rotor .....	30
3.5.1 Material selection .....	31
3.6 Number of blades .....	31
3.7 Tip Speed Ratio, TSR ( $\lambda$ ).....	31
3.8 Selection of Pump .....	32
CHAPTER FOUR.....	33
MODELLING AND NUMERICAL ANALYSIS.....	33
4.1 Geometry and Computational Domain .....	33
4.2 Modeling of the Savonius Wind Turbine.....	37
4.3 Simulation Procedure .....	41
4.3.1 Turbulence model.....	41
CHAPTER FIVE .....	45
RESULT AND DISCUSSION .....	45
5.1 Graphical Displays .....	45
5.1.1 Velocity distribution.....	45
5.1.2 Pressure distribution .....	48
5.2 Effect of Aspect Ratio, AR .....	50
5.3 Effect of adding fins to the savonius rotor on the power coefficient .....	50
5.4 Comparative analysis of Drag and Lift Coefficient .....	51

Performance Analysis and Simulation of Savonius Wind Turbine for Small-Scale Water Pumping System

---

CHAPTER SIX.....	52
6.1 CONCLUSION AND RECOMMENDATION.....	52
6.1.1 Conclusion.....	52
6.1.2 Recommendation .....	54
REFERENCE.....	55
APPENDIX.....	58



## LIST OF FIGURES

FIGURE 1. 1 GLOBAL CUMULATIVE WIND POWER CAPACITY WORLDWIDE (WENEHENUBUN, SAPUTRA, AND SUTANTO, 2015) .....	2
FIGURE 1. 2 TOTAL ENERGY SUPPLY IN ETHIOPIA IN 2014 [INTERNATIONAL ENERGY AGENCY]....	2
FIGURE 1. 3 ANNUAL WIND SPEED IN ETHIOPIA[ETHIOPIA ENERGY SITUATION] .....	3
FIGURE 1. 5 CONFIGURATION OF SAVONIUS WIND TURBINE(MAHMOUD <i>ET AL.</i> , 2012A).....	6
FIGURE 1. 6 CENTRIFUGAL PUMP (B.U.PAI WILEY, 2013).....	8
FIGURE 1. 7 POSITIVEDISPLACEMENTS (B.U.PAI WILEY, 2013).....	8
FIGURE 2. 1 SAVONIUS WIND TURBINE FOR THE APPLICATION OF WATER PUMPING .....	13
(ARGAW, FOSTER, AND ELLIS, 2003).....	13
FIGURE 2. 2 EFFECTS OF ENDPLATES ON THE PERFORMANCE OF SAVONIUS WIND TURBINE_(AKWA, VIELMO AND PETRY, 2012) .....	15
FIGURE 2. 3 SAVONIUS ROTOR WITH DIFFERENT ASPECT RATIOS (BRUSCA, LANZAFAME AND MESSINA, 2014) .....	16
FIGURE 2. 4 REPRESENTATION OF BLADE SPACING AND OVERLA (SANUSI ET AL., 2016).....	16
FIGURE 2. 5 TWO AND THREE BLADES (DUMITRESCU <i>ET AL.</i> , 2015) .....	18
FIGURE 2. 6 INTERFACE OF SHAFT (HADI ALI, 2013).....	19
FIGURE 3. 1 DODOTAMAP(GOOGLE MAP).....	22
FIGURE 3. 2 TWO BLADED S-VAWT WITH THE DRAG FORCES (HADI ALI, 2013) .....	23
FIGURE 3. 3 FLOW CHARTS OF THE METHODOLOGY ADOPTED FOR THIS STUDY .....	25
FIGURE 3. 4 DISTRIBUTION OF AVERAGE WIND SPEED (M/S) IN ETHIOPIA AT HEIGHTSOF 50 M AND 10 M RESPECTIVELY, FROM 2000 TO 2009(MISRAK G. ET AL., 2015) .....	25
FIGURE 3. 3 CURVES OF CP- $\lambda$ FOR DIFFERENT WIND TURBINES (WENEHENUBUN, SAPUTRA, AND SUTANTO, 2015).....	29
FIGURE 3. 4 SAVONIUS ROTOR WITH DIFFERENT ASPECT RATIO (BRUSCA, LANZAFAME AND MESSINA, 2014) .....	30
FIGURE 3. 5 POWER CURVE GRAPH .....	32
FIGURE 4. 1 SAVONIUS BLADES (A) WITHOUT FIN (B) WITH 1 FIN (C) WITH 2 FIN .....	34
FIGURE 4. 2 COMPUTATIONAL DOMAIN IMMERSD SAVONIUS ROTOR IN OPEN CHANNEL .....	34
FIGURE 4. 3 SAVONIUS WIND TURBINE MODELING DOMAIN .....	35

Performance Analysis and Simulation of Savonius Wind Turbine for Small-Scale Water Pumping System

---

FIGURE 4. 4 BOUNDARY CONDITIONS FOR CFD ANALYSIS ..... 36

FIGURE 4. 5 MESHING RESULTS OF SAVONIUS WIND TURBINE ..... 39

FIGURE 4. 6 MESH INDEPENDENCY GRAPHS FOR MEDIUM, FINE AND COURSE SPAN ANGLE CENTER RESPECTIVELY ..... 40

FIGURE 4. 7 FLOWCHART SIMULATION ..... 44

FIGURE 5. 1 VELOCITY DISTRIBUTION FOR (A) WITHOUT FIN (B) 1 FIN (C) 2 FINS ..... 46

FIGURE 5. 2 VELOCITY DISTRIBUTION DONE BY (RIDWAN, SETYAWAN AND SETIYONO, 2019) (A) WITHOUT FIN (B) 1 FIN (C) 2 FINS ..... 47

FIGURE 5. 3 PRESSURE DISTRIBUTION OF SAVONIUS ROTOR WITHOUT FIN ..... 48

FIGURE 5. 4 PRESSURE DISTRIBUTION (A) WITH ONE FIN (B) WITH TWO FINS ..... 49

FIGURE 5. 5 CUT PLOT PRESSURE BY (RIDWAN, SETYAWAN AND SETIYONO, 2019) (A) WITHOUT FIN (B) 1 FIN (C) 2 FINS ..... 50

FIGURE 5. 6 COMPARISON OF POWER COEFFICIENT FOR BLADES WITHOUT A FIN, 1 FIN, AND 2 FINS ADDITION ..... 51

LIST OF TABLES

TABLE 3. 1 WIND SPEED [NATIONAL METROLOGY AGENCY OF ETHIOPIA, NMAE]..... 25

TABLE 3. 2 MONTHLY TEMPERATURE DISTRIBUTION ..... 26  
(NATIONAL METROLOGY AGENCY OF ETHIOPIA, NMA) ..... 26

TABLE 3. 3 PRACTICAL EFFICIENCIES OF VARIOUS MECHANICAL DEVICES (BURTON *ET AL.*, 2011)28

TABLE 3. 4 EFFICIENCY COMPARISON (CONTENTS, NO DATE) ..... 28

TABLE 4. 1 DESIGN PARAMETER FOR THE SAVONIUS WIND TURBINE..... 33

TABLE 4. 2 BOUNDARY CONDITIONS FOR NUMERICAL ANALYSIS..... 36

TABLE 4. 3 SIZING MODEL ..... 37

TABLE 4. 4 MESH QUALITIES OF THE STUDY ..... 38

TABLE 6. 1 COMPARISON OF PRESENT STUDIES WITH THE PREVIOUS STUDIES..... 52

## NOMENCLATURE

<b>Symbols</b>	<b>Description</b>
HAWTs	Horizontal Axis Wind Turbines
VAWTs	Vertical Axis Wind Turbines
D	Rotor diameter
R	Rotor radius
H	Rotor height
t	Blade thickness
$A_s$	The cross-sectional area of the rotor
H	Head
Q	Flow rate
$\lambda$	Tip Speed Ratio
$\rho$	Density of air
V	Wind speed
AR	Aspect Ratio
$T_g$	Teeth of Gear
$T_p$	Teeth of Pinion
m	Module
w	Face width
$C_t$	Torque coefficient
$C_p$	Power coefficient
k	Turbulent kinetic energy
RSM	Reynolds Stress Model
SIMPLE	Semi-Implicit Method for Pressure-Linked Equations
SST	Shear Stress Transport
URANS	Unsteady Reynolds-averaged Navier-Stokes
$\varepsilon$	Turbulent dissipation rate
ASME	American Society of Mechanical Engineers
BHN	Brinell Hardness Numbe

## CHAPTER ONE

### INTRODUCTION

#### 1.1 Background

Climate change is the world's most serious and life-threatening environmental concern. The hothouse effect, which is caused by human activity, such as the burning of fossil fuels like coal, oil, and gas for energy, causes global temperatures to rise, leading to more severe weather patterns like floods, droughts, and storms, as well as rising sea levels and threats to entire ecosystems. The world approves an energy conversion program, in which fossil fuels are replaced with renewable energy sources to reduce CO<sub>2</sub> emissions (Talur, Kumar, and Madhusudhan, 2015). We transform all of our energy into heat, which is then radiated into space. From one point of view, the diffusion of renewable energy into the energy system of human settlements on the ground is around 100 percent. Environmental heat associated with atmospheric phenomena, which captures solar power and stores it inside a surface-near sheet of topsoil and atmosphere encircling the Earth (Talur, Kumar, and Madhusudhan, 2015), dominates the energy system as seen by the world's inhabitants. Renewable energy foundations have grown in popularity and output over the last decade.

Wind energy is an environmentally friendly energy source with huge potential to meet people's energy needs and alleviate climate change caused by greenhouse gases emitted by fossil fuel combustion. It is estimated that the earth's wind energy provides approximately 10 million Megawatts of energy. The International Energy Agency (IEA) shows the cumulative global installed wind power capacity based on the forecast in the 2004 World Energy Outlook report (Mahmoud *et al.*, 2012a).

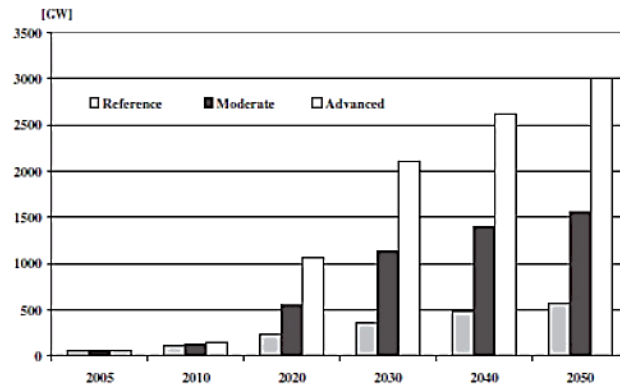


Figure 1. 1 Global cumulative wind power capacity worldwide (Wenehenubun, Saputra, and Sutanto, 2015)

Ethiopia has some types of renewable energy sources. Those are hydropower, wind energy, geothermal energy, solar energy, biofuels, and biomass. Biofuels cover most of Ethiopia's energy supply [Ethiopian Energy Situation].

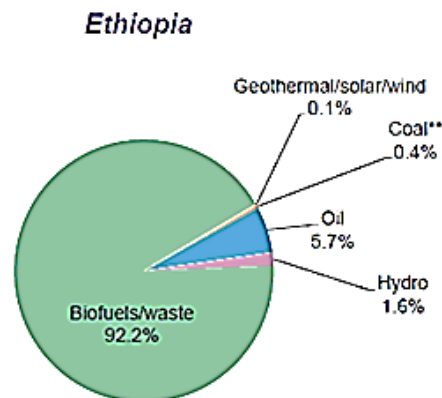


Figure 1. 2 Total energy supply in Ethiopia in 2014 [International Energy Agency]

The majority of air movement is caused by wind, which is the flow of gases on an extremely large scale. Solar radiation is the passage of gases or charged particles from the sun across space, whereas planetary wind is the out-gassing of sunlit chemical components from the atmosphere of a planet into space (Bisen and Wasnik, 2019). Wind energy is one of the renewable energy sources that has gained a lot of attention and has grown rapidly, and it is one of the alternative trustworthy energy resources utilized to lift water (Lukiyanto, 2016). A wind turbine is a mechanism that converts mechanical energy from kinetic energy.

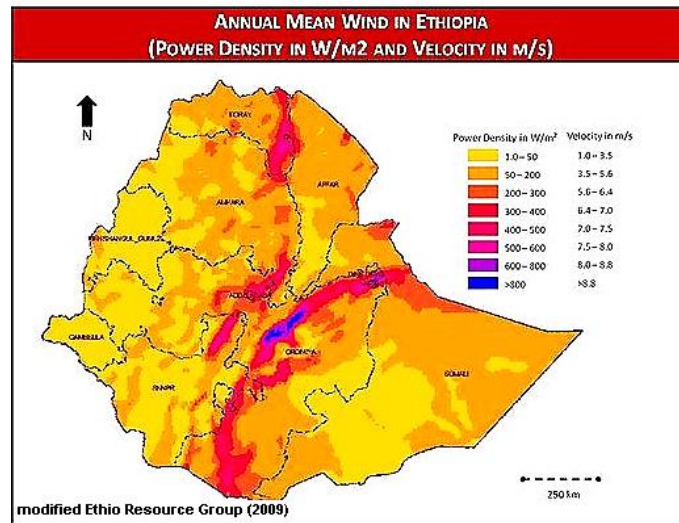


Figure 1. 3 Annual wind speed in Ethiopia[Ethiopia Energy Situation]

### Types of wind turbines

Wind turbines are classified based on wind direction,

➤ Drag-type wind turbine

The wind exerts a force in the direction that it is blowing in a drag-type turbine. That is, it merely pushes against a surface, much as a ship sailing against the wind.

➤ Lift-type (with vertical or horizontal axes)

The wind creates a force that is perpendicular to the direction it is blowing in this type. The horizontal-axis, lift-type propeller wind turbines are the most common. All lift-type turbines are like sailboats sailing against the wind.

➤ Magnus effect wind plants

When a pitcher throws a curve, it causes the ball to spin, causing an asymmetry: one side of the ball moves quicker with the air than the other, generating a lift that changes the ball's trajectory. When a vertical spinning cylinder is exposed to the wind, it produces a similar effect. The resulting force has moved sailboats and wind machines, which is normal for the wind direction.

➤ Vortex wind plants

By forcing the wind to enter tangentially through a vertical slit into a vertical hollow cylinder, energy can be extracted from the wind. As a result, the air inside is forced to gyrate, resulting in a radial pressure gradient due to the centrifugal force. Because the core of this air column is at a lower pressure than the surrounding atmosphere, it sucks outside air through the cylinder's bottom holes. The incoming air powers a turbine that is connected to a generator. The spinning air escapes the cylinder through the open top, generating a vortex that is constantly pushed away by the wind.

1. Wind turbines are also classified according to their rotational axis.

➤ Horizontal axis wind turbine (HAWT)

In a horizontal shaft wind turbine, the rotor's axis is aligned with the horizontal axis, which may be adjusted to be parallel to the direction of the wind stream. Glass fiber reinforced plastic and aluminum, cast iron, and carbon fiber are the most common materials utilized for blades. On windmills, a yaw mechanism rotates the nacelle along its vertical axis to keep it facing the wind.

➤ Vertical axis wind turbine (VAWT)

VAWTs often operate closer to the ground, which has the advantage of allowing heavy equipment, like the gearbox and generator, to be placed closer to the ground level. However, because the winds are weaker near ground level, less power is generated for an identical wind and capture area.

VAWTs are

- Because the rotor is the main moving component and the more sophisticated pieces like the gearbox and generator are positioned at the base of the wind turbine, it is small, silent, and simple to install.
- Can take the wind from any direction and operate effectively under high-turbulence circumstances.
- Due to the constant cross-section blades, manufacturing a VAWT is easier than a HAWT. As a result, they are well suited for household use.



### Darrieus type (D-VAWT)

Due to the lift force produced by the spinning airfoils, the Darrieus wind turbine is a VAWT that rotates around a central axis.

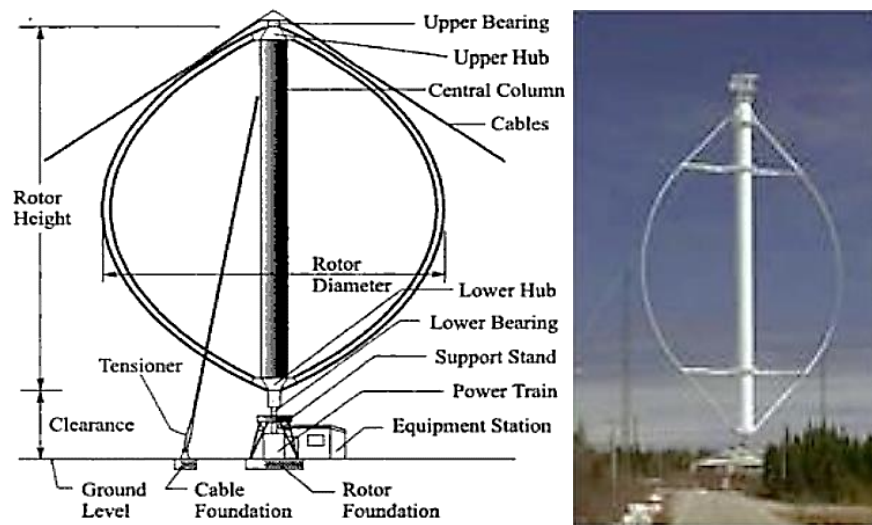


Figure 1.4 Configuration of Darrieus wind turbine (Talur, Kumar, and Madhusudhan, 2015)

### Savonius Types (S-VAWT)

Sigurd J. Savonius originally invented the Savonius type wind turbine, also called S-rotor, in 1931. The turbine is made of two or more half cylinders and then moves the semi-cylinder surfaces sideways along the cutting plane like the letter S. The semicircular surfaces, called blades or buckets, are mounted on a vertical axis perpendicular to the wind direction with the gap at the axis between the blades or the overlap. The Savonius turbine works like a cup anemometer or a drag-based device. The ratio of the blade tip speed to wind speed is less than one because the returning blades on the downwind side can never travel faster than the wind (Wenehenubun, Saputra, and Sutanto, 2015).

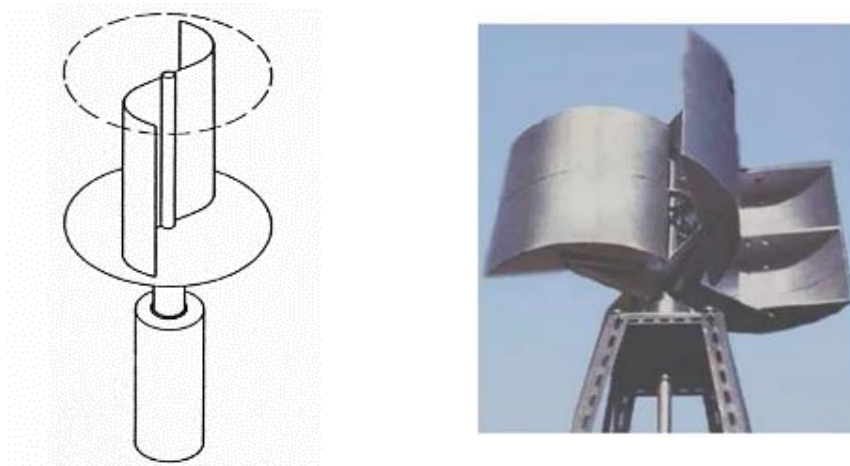


Figure 1.5 Configuration of Savonius wind turbine(Mahmoud *et al.*, 2012a)

Savonius wind turbines are best suitable for pumping water, grinding grain, and electricity for which slow rotation and high torque are desirable.

WEWPS (wind energy water pumping systems) is one option for overcoming water scarcity and availability. WEWPS can operate independently with other renewable energy resources such as solar photovoltaic water pumping systems that are available in the vicinity (SPWPS). Even before wind generators that convert wind energy into electricity, WEWPS had been utilized for irrigation and supporting agricultural activities. The key advantages of WEWPS are (B *et al.*, 2018)

- ✓ They are cost-effective
- ✓ Ecologically friend
- ✓ They are installed and maintained by the user for small or medium-sized wind turbines.

Natural slopes, rise to a higher elevation, and pumps and pressured pipelines, frequently transport water. Water lifting devices range from simple hand pumps to extremely efficient pumps powered by electric, gasoline, or diesel motors (B *et al.*, 2018). A pump is a device that is used to transfer fluid by converting the fluid's mechanical energy into hydraulic energy.

## Pumps

A pump is a device, which converts mechanical energy to hydraulic energy. They have usually two major functions

- Transporting fluid from lower elevation to higher elevation or some finite distance horizontally overcoming the friction loss in pipes.
- Developing very high pressure as in hydraulic machines.

Pumps are classed based on

- ✓ The principle by which energy is added to the fluid
- ✓ According to the applications they serve
- ✓ The materials they are made of
- ✓ The liquids they handle

All pump types fall into one of the following two groups.

- Centrifugal (dynamic) pump

A centrifugal pump is a machine used to lift liquid from a lower level to a higher level. The input of the centrifugal pump is the mechanical energy in the form of torque on its rotating shaft. The output of the pump is the increased energy of the liquid in the form of the pressure or momentum (or both) of the liquid being lifted. Thus, the centrifugal pump converts mechanical energy into the energy of the liquid. Centrifugal pumps handle a variety of liquid chemicals, different types of oils, slurries, etc. The main drawback is to get very high-pressure ratios is not possible (B.U.Pai Wiley, 2013)

Advantages

- ✓ The flow process is continuous and not periodic.
- ✓ The parts are few in number, simple, their manufacture requires less care, and they are less costly.
- ✓ The operating and maintenance cost is low.
- ✓ The hydraulic, volumetric, mechanical, and overall efficiencies are high.
- ✓ Control of the flow of fluid is very easy.

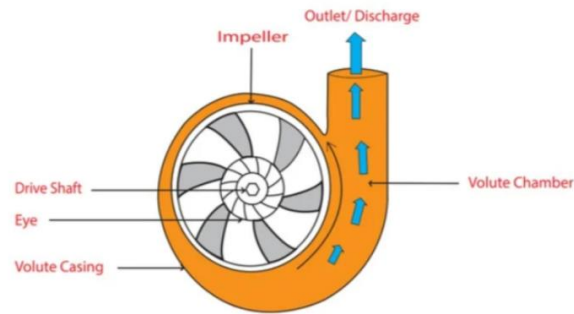


Figure 1. 6 Centrifugal pump (B.U.Pai Wiley, 2013)

➤ Positive displacement pump

Universally used for fluid power as in hydraulic machine and operates by forcing a fixed volume of fluid from the inlet pressure section of the pump into the discharge zone of the pump. Add energy directly to a movable boundary, which imparts the energy to the fluid.

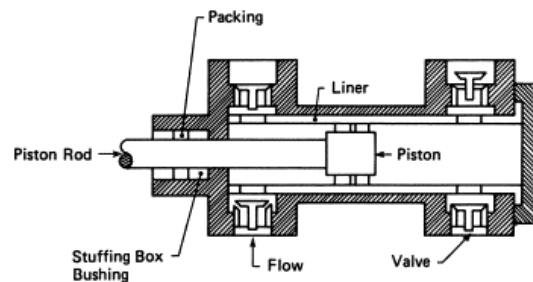


Figure 1. 7 Positivedisplacements (B.U.Pai Wiley, 2013)

Types of positive displacement

- Rotary pumps: Gears, lobes, or screw-type shafts mate to operate.  
E.g., Vane, piston, gear, etc.
- Reciprocating pumps: To displace fluid, use pistons, plungers, or diaphragms.  
E.g., Steam, power, controlled volume, etc.

## 1.2 Statement of the Problem

Water is the life of every living things. It can be accessed in different ways for different domestic services, agriculture, and horticulture. Now adays renewable energies are used for irrigation purposes in addition to producing power. The feasibility of S-VAWT energies for agriculture, and horticulture purposes was studied by many researchers. However it is limited due to its lower efficiency and performance. The turbine operates at lower wind speed which indirectly decreases its output power compared to other types of the turbine. Aspect ratio, and other parameters were used to modify the Savonius turbine but each parameter have their own impact on the turbine's blade and power output.

## 1.3 Objectives

### 1.3.1 General Objective

The main objective is to enhance the performance and simulation of the Savonius wind turbine for a small-scale water pumping system.

### 1.3.2 Specific Objectives

- To design the blades of the Savonius wind turbine
- To study and evaluate the effect aspect ratio and addition of fins on the performance of the blades
- To model the 3D geometry and simulate the Savonius wind turbine using ANSYS 19.2
- To compare the results with others researchers work

#### 1.4 Justification of the study

In Ethiopia, mostly in rural areas, people use water from a river, rain, and different sources for their daily activities. In most areas, water comes from far distances using man-powered or other technologies like the pump. However, because of their economic status, they prefer manpower, which is tedious. To prove this problem, the research justifies that using renewable energy (wind energy with Savonius wind turbine) simplifies the problem for societies.

#### 1.5 Scope of the study

With the increase in the number of populations in Ethiopia, demand for water in everyday activities is increasing in both urban and rural areas, especially for irrigation. Dodota is one of the rural areas in which peoples are dependent upon irrigation. This study analyzes the performance of the Savonius wind turbine for small-scale water pumping by taking data from the National Metrology Agency of Ethiopia (NMA) for the time ranging from 2015 to 2017 G.C, and parameter study with addition of fin to the shape of S-VAWT were investigated. The study is restricted only to irrigation purposes. Finally, the study involves the design and performance analysis of the Savonius wind turbine with limitations to the Dodota area.

## CHAPTER TWO

### LITERATURE REVIEW

#### 2.1 Wind energy

There is wind everywhere. When air moves from areas of high pressure to areas of low pressure, it creates a vortex. When this mass of air moves, it contains the energy required to pump water for irrigation and generate electricity using wind turbines.

#### Types of Wind Turbines

Based on their blade configuration and operation, there are two basic types of wind turbines.

- Horizontal Axis Wind Turbines (HAWT)

HAWTs have a series of blades that rotate along an axis parallel to the flow direction and sit atop a tall tower. By generating lift, the blades extract energy from the wind, resulting in a net torque about the axis of rotation. Each blade is adjusted to maintain an appropriate angle of attack for maximum power extraction for a particular wind speed to complete this duty efficiently.

- Vertical Axis Wind Turbines (VAWT)

The VAWT wind turbine revolves around a perpendicular axis to the oncoming flow. VAWTs are becoming more popular as people become more interested in personal green energy options. As a means of producing local and personal wind energy, VAWTs target individual residences, farms, or small residential areas. Due to the constant cross-section blades, manufacturing a VAWT is significantly easier than a HAWT. There are two types of VAWTs.

- ✓ Darrieus wind turbine

The lift produced by the rotating airfoils causes a VAWT type to rotate around a central axis. Lift force is used to generate energy.

- ✓ Savonius wind turbine

The drag force exerted by the blades causes a VAWT type to rotate. The wind blows against a surface, similar to an open sail, and it works because the drag force on the cylinder's concave or face is larger than the drag force on the closed or convex section. The wind becomes trapped as it

contacts the concave portion of the blade (the bucket) and drives the blade around, advancing the next bucket into place. This will continue as long as the wind blows and the friction of the shaft around which the blades rotate is overcome. A Savonius rotor normally rotates at the same speed as the free stream velocity, or with a tip speed ratio of one.

#### Merits

- Simple and cheap construction
- Relatively low operating speeds
- Low noise
- High starting torque
- Ability to accept wind from any direction
- Requires lower space

#### Demerits

- Lower efficiency

S-VAWTs are best suitable for

- ✓ Pumping water
- ✓ Grinding grain and
- ✓ Electricity (power production)

One alternative for overcoming water scarcity and availability is WEWPS (wind energy water pumping systems). WEWPS can run on its own or in conjunction with other renewable energy sources such as solar photovoltaic water pumping systems in the area (SPWPS). WEWPS had been used for irrigation and agricultural support long before wind generators converted wind energy into electricity.





Figure 2. 1 Savonius wind turbine for the application of water pumping (Argaw, Foster, and Ellis, 2003)

(Argaw, Foster, and Ellis, 2003) was compared to traditional pumping systems by determining the proper measurement of a PV or wind pumping system, which includes the water tank and necessitates a careful evaluation of each component and the entire system. Water tanks typically cost less than PV arrays or wind turbines, and instead of oversizing the PV or wind pumping system at a much greater cost, water is frequently saved for low radiation or less windy days by installing a much larger cistern. Steel, PVC, fiberglass, concrete, or masonry are commonly used as water storage tanks for home water devices. For PV or wind systems, steel, fiberglass, and PVC water tanks are typically used. Small to medium-sized concrete and masonry water tanks can also be used for wind and PV projects, but they are more expensive than ready-made fiberglass, steel, and PVC water tanks. For large water system projects, larger concrete and masonry water tanks are usually more practical. When choosing a material for water tanks, take into account the location and topography.

(Misrak G. et al., 2015) studied guide and diesel engine water pumping and created a wind water pump to provide drinking water to Ethiopian rural areas. The MATLAB software is used to simulate the entire performance of the selected windpump. Finally, based on the economic situation and life cycle cost, it was determined that windmill water pumping structures are more

practical than diesel-based systems. (Lukiyanto, 2016) looked into a centrifugal reaction pump, a Savonius windmill, and a transmission that connected the two as WEWPS. As automatic on-off devices, the centrifugal reaction pump was modified by swapping the fixed and sliding orifices with a double U pipe structure. The Savonius windmill was chosen because of its high beginning torque, moderate peak power output, and ability to accept wind from any direction. The transmission of shaft power from the windmill shaft to the pump shaft is required. Low wind speeds should be used to determine the proper transmission ratio for WEWPS.

Because some crops require a large amount of water for a short time, crop irrigation water requirements are seasonal. Irrigation water pumps are unique in that they require a big volume of water to operate. As a result, for surface water sources or shallow wells with high yields, wind and solar-powered irrigation pumps are frequently advised. In this environment, producing high-value cash crops is advantageous, making such systems economically viable. Irrigation water consumption varies by crop and is influenced by factors such as climate.

## 2.2 Factors affecting the performance of S-VAWTs (Akwa, Vielmo, and Petry, 2012)

### a. Endplate

The simplest accessory that can be added to a Savonius turbine to improve its performance is an endplate. When endplates are added to a Savonius turbine, the maximum averaged power coefficient,  $C_p$  averaged, can be considerably increased. Higher tip speed ratios further improve the efficiency of the turbine. (Mahmoud *et al.*, 2012b) conduct an experiment performance of the Savonius rotor. He discriminated between different blades to establish the most effective operation conditions. He compared rotors with and without endplates, single and double stage rotors, and rotors with and without overlap ratio once again. Finally, he decides that the Savonius wind turbine with two blades and an endplate rotor is the most efficient. The performance of the double stage rotor is better. Rotors with a low overlap ratio perform better than those with a high overlap ratio. He concluded that the coefficient of power grows as the aspect ratio increases.

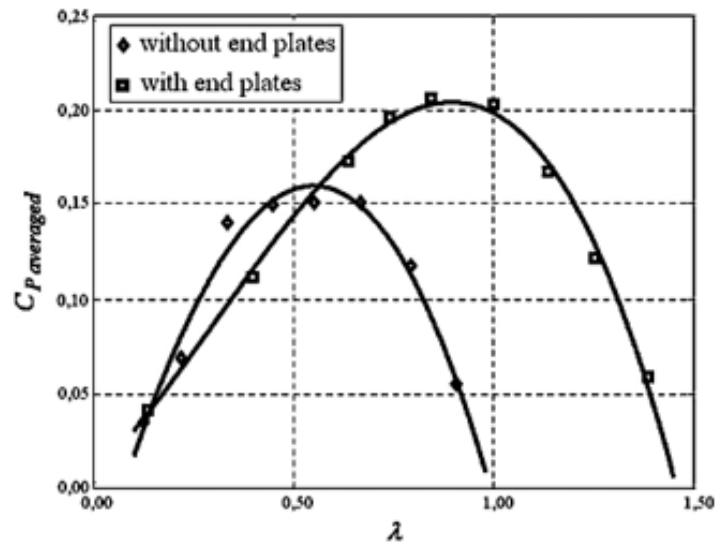


Figure 2. 2 Effects of endplates on the performance of Savonius wind turbine  
(Akwa, Vielmo and Petry, 2012)

The plates at the turbine end prevent air from escaping from the concave side of the buckets into the external flow, maintaining an acceptable pressure difference between the concave and convex sides of the buckets throughout the rotor's height. The appropriate size of this item has been agreed upon in the literature. In relation to the height of Aboutine, a thin layer is advised. The recommended endplate diameter is comparable to 1.1 times the rotor diameter. Endplates with extremely large diameters can significantly increase rotor inertia.

#### b. Aspect Ratio

The Aspect Ratio, AR, of a turbine is calculated by multiplying the blade height, H, by its diameter, D. Due to the action of the bucket tips, Savonius rotors with high aspect ratios have low losses. Reynolds numbers change as the aspect ratio of a vertical-axis wind turbine changes. According to the majority of research, the aspect ratio has an impact on the turbine's efficiency. The aspect ratio of the rotor should be as minimal as feasible to enhance the power coefficient. When the aspect ratio, AR, is less than one, good efficiency is achieved (Brusca, Lanzafame and Messina, 2014).

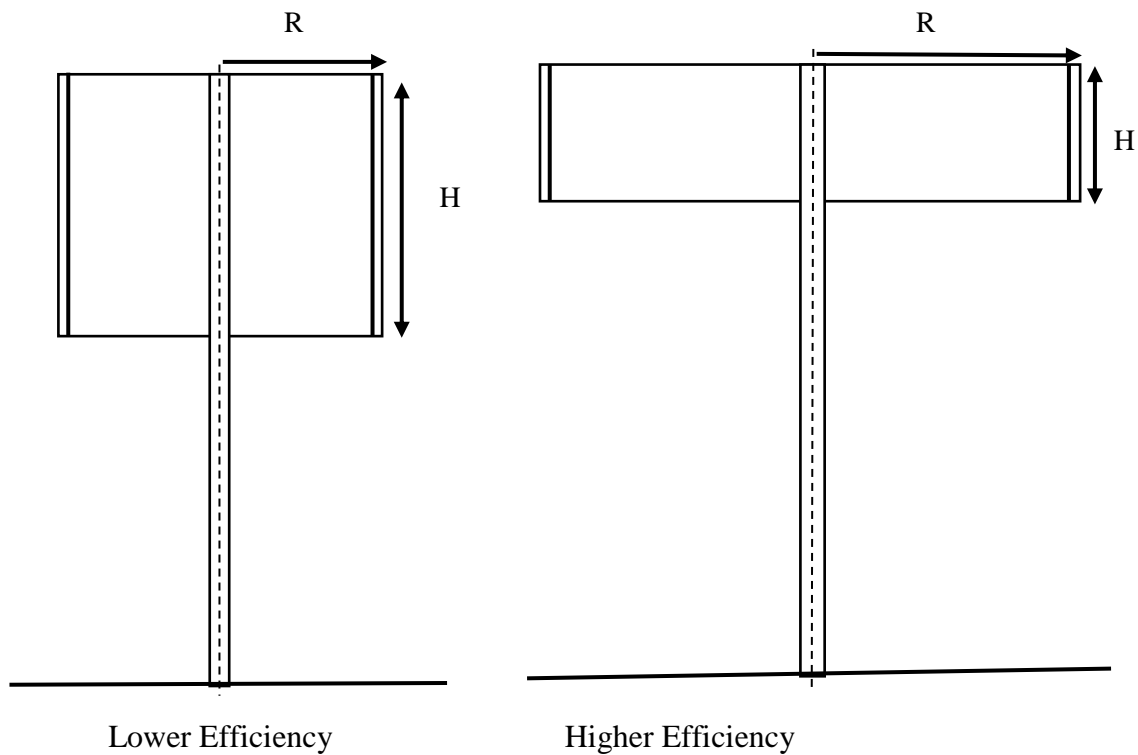


Figure 2. 3 Savonius rotor with different Aspect Ratios  
(Brusca, Lanzafame and Messina, 2014)

c. Influence of blade spacing and overlap

Several Savonius turbine experiments focused on determining the impact of blade spacing and overlap on rotor performance. The majority of studies conclude that a Savonius wind rotor with semi-circular profile blades performs best with a null blade spacing. The air does not focus sufficiently on the concave region of the returning blades when the blade spacing is large, limiting the turbine's output.

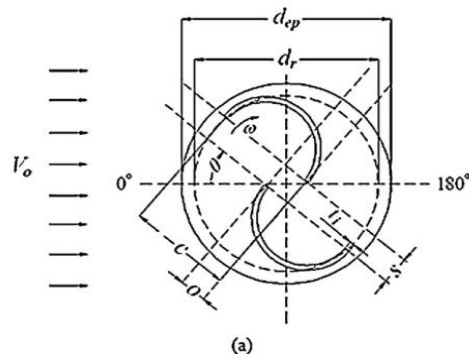


Figure 2. 4 Representation of blade spacing and overlap  
(Sanusi et al., 2016)

d. Number of blades and rotor stages

The range of values for angular locations of the advancing bucket where the rotor moment is low reduces as the number of blades grows because the chance of a rotor bucket being in a position favorable to the extraction of momentum from airflow increases. The addition of buckets to a Savonius rotor, on the other hand, reduces the maximum averaged power and moment coefficients as well as the angular positions. This happens because a bucket deflects airflow that would otherwise focus on the next bucket, which then deflects airflow that would otherwise focus on the bucket after it. This results in a "cascade effect," in which the performance of one bucket influences the performance of the next. As a result, the rotor converts less of the energy released by the moving air into mechanical energy. The highest averaged power coefficient of a Savonius rotor with two buckets is thus higher than the maximum averaged power coefficient of a Savonius rotor with numerous buckets.

(Wenehenubun, Saputra and Sutanto, 2015) conducted research to see how the number of blades affects the performance of the Savonius wind turbine type. The experiment uses two, three, or four blades to determine the tip speed ratio, torque, and power coefficient as a function of wind speed. The ANSYS 13.0 software simulation shows the pressure distribution. Finally, the findings revealed that the number of blades on a wind turbine affects its total performance. The four-bladed Savonius variant provides excellent overall performance at a high tip speed ratio.

(Dumitrescu *et al.*, 2015) CFD methods were used to examine the flow-through Savonius wind axis turbine mathematically. Despite its low efficiency, the Savonius wind turbine may be used for water extraction due to its strong torque at low wind speeds. The unsteady flow around the vertical axis turbine was usually evaluated using two-dimensional models. Finally, he decided that it may be employed in agricultural domains, such as crop irrigation, where this gadget extracts water.

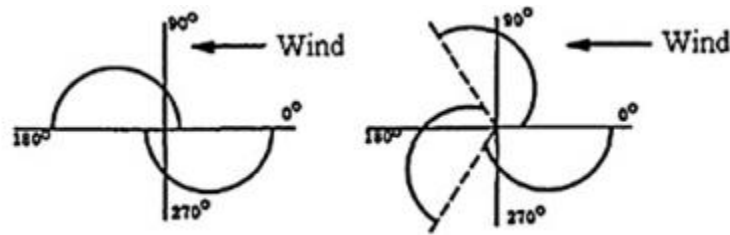


Figure 2. 5 Two and Three blades  
(Dumitrescu *et al.*, 2015)

e. Buckets and rotor shapes influence

(Zhou and Rempfer, 2013) has calculated the non-linear two-dimensional unsteady flow over standard Savonius and Bach rotor classes and developed a modeling approach for estimating their aerodynamic performance. Star-CCM<sup>+</sup> is used to do the simulations. A moving mesh is used to tackle the blade movement problem. A comparison of the two types of rotors was conducted, and the results of numerical simulations were compared to experimental data. The Bach-kind rotor has been proven to have better overall torque and power coefficient performance than the traditional Savonius-kind rotor.

(Tian *et al.*, 2015) by evaluating altered Savonius wind turbines with innovative blade shapes to boost the turbine's power coefficient, the numerical system analysis is proven alongside the current experimental knowledge in a visual manner. The transient computational fluid movement was used to investigate the effect of blade fullness on the capacity of a two-bladed Savonius wind turbine (CFD). The relationship between blade fullness and turbine performance is quantified, with a blade fullness of one yielding the maximum coefficient of power, 0.2573. This power coefficient is 10.98% higher than a standard Savonius turbine.

(Sanusi *et al.*, 2016) offered to resolve the effect of blade combination on the Savonius wind turbine's performance. The traditional model is merged with the concave elliptical model, which does not affect the lack of complexity, construction, or the cost of manufacturing turbine rotors. The experiment was carried out in a rotor prototype's open-jet wind tunnel with three different blade types of the same dimension. The result demonstrates that at a tip speed ratio of 0.79, the connected blade outperforms the traditional blade in terms of power coefficient maximum performance by 11 percent.

f. Interference of shaft and other accessories

A passing shaft, according to various prior research on the performance of Savonius wind turbines, causes airflow interference due to the space between the rotor buckets. This has the consequence of lowering efficiency. A passing shaft, on the other hand, can be used as an add-on to give the wind turbine frame more rigidity. In this situation, the bucket spacing and overlap should be increased to compensate for the shaft's blockage effect on airflow (Hadi Ali, 2013).

To boost the averaged power coefficient of a Savonius wind turbine, certain accessories can be added. Valves that only allow air to move from the convex to the concave side of a bucket reduce bucket drag when acting as a returning bucket, resulting in a 0.26 to 0.31 improvement in the averaged power coefficient for a two-stage turbine with three semi-circular profile buckets.

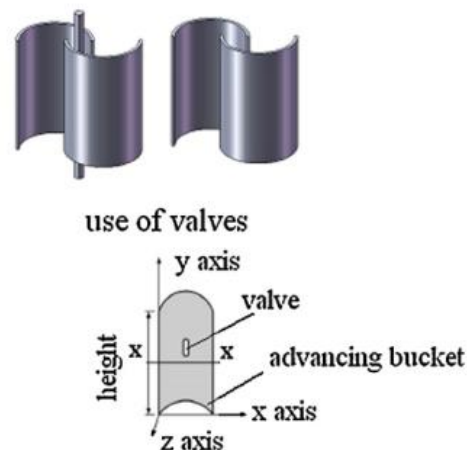


Figure 2. 6 Interface of shaft  
(Hadi Ali, 2013)

g. Influence of Reynolds number and turbulence intensity

The phenomenon of boundary layer separation on the rotor buckets is affected by increasing the Reynolds number. Increases in this quantity slow the separation of the boundary layer on the convex side of the buckets, especially for angular positions near 0 or 180°. The pressure drag on the returning bucket is reduced by delaying the boundary layer separation. This is due to higher

pressure recovery, which increases the lifting force's contribution to the resultant force for certain angular positions while also increasing the rotor's moment.

Turbulence intensity, which describes the quality of the airflow surrounding the device, is another aspect that may affect the performance of a Savonius wind turbine. Wind turbine performance is influenced by low-quality airflow or turbulent flow. To improve the effectiveness of output power, (Samiran *et al.*, 2014) introduced the Savonius rotor planning enhancement. The goal of the study was to see how geometrical arrangement affected the rotor's overall performance in terms of coefficient of torque, energy, and energy production. To study the flow characteristic and calculate the torque coefficient of all rotor designs, CFD simulation is utilized.

The commercial software tool ANSYS-Fluent is used to solve the continuity and Reynolds Averaged Navier-Stokes (RANS) equations, as well as the realizable k-epsilon turbulence model. The derived results for the traditional two-bladed Savonius rotor are compatible with experimental results.

#### h. Influence of stators

Stators are fixed components that are added to turbines to divert or concentrate flow in a specific direction. A blade, for example, deflects flow onto the concave side of the advancing rotor bucket, minimizing the negative moment exerted by the returning bucket and improving the device's output net power. The savonius wind turbine's performance is also improved by the addition of fins. The addition of a fin to the turbine blades increased the power generated by the Savonius wind turbine (Pamungkas *et al.*, 2018). When fins were added, the power increased when compared to the power without fins. (Utomo, Tjahjana and Hadi, 2018) also found that adding a fin to the Savonius wind turbine increases wind turbine efficiency by creating a positive drag force. According to the experiments, employing fin yields the highest  $C_p$  when compared to not utilizing fin. On Savonius wind turbine modifications, increasing the fin area can help give maximum drag force.



### 2.3 Improvements made

Different research deals with the way to improve the performances of S-VAWTs using different ways. Those improvements were on:

- ✓ Blade shapes
- ✓ Number of blades
- ✓ Stage of rotor
- ✓ Combination of blade types
- ✓ Addition of fins
- ✓ Varying parameters (aspect ratio, tip speed ratio, twist-angle, chord ratio, etc.)

### 2.4 Literature Conclusion and Research Gap

S-VAWTs have limited applicability due to their poor efficiency; nevertheless, some researchers have found a method to increase its performance and efficiency by modifying the parameters listed earlier, even though each has its own set of limitations. The gap in literature is that the researcher only considers some parameters with limited outputs to increase the efficiency of S-VAWTs. The result shows the blades without fin at an aspect ratio of 1, the increment in coefficient of power is only 9.2%. The research aims to improve the performance of the Savonius wind turbine by adding fins to the rotor of the blades, minimizing the aspect ratio's value, and avoiding the blade space.

## CHAPTER THREE

### DESIGN AND METHODOLOGY

#### 3.1 Study Area

This study was conducted for Dodota woreda, Arsi Zone ( $8^{\circ}14'60.00''$  N and  $39^{\circ}19'60.00''$  E), which is located in the Arsi Zone of Southeast Ethiopia. Addis Ababa is 125 kilometers away. The elevation at the site is 1680 m above sea level. The total area covered by Dodota is estimated at around  $300 \text{ Km}^2$  (Poluha *et al.*, 1990). The data was undertaken during the dry season (December–May) from 2015 to 2017. The major soil type of the study area was classified as Andosol which has a texture of clay loam. The crops which could be grown are carrot, beetroot, potato, onion, cabbage, and maize (Poluha *et al.*, 1990).

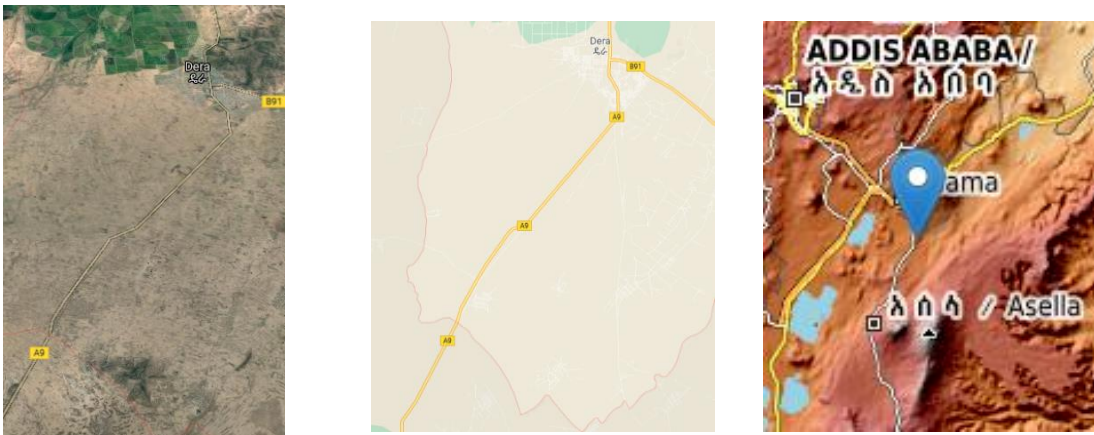


Figure 3. 1 DodotaMap(Google Map)

#### 3.2 Research Strategies

##### 3.2.1 Research strategy

Experiments, surveys, archival analysis, histories, and case studies are the five major research methodologies used in research. From December 2015 until the end of May 2016, a case study of the Dodota spate irrigation system was conducted. Following a quick assessment of the location, the system, design, and construction were thoroughly examined. The data acquired might be quantitative or qualitative, however, for this study, qualitative data is the most important factor to consider. To check and validate, multiple resources were used.

Information was acquired through personal interviews in addition to secondary data and field observations. The irrigation system's users were questioned about how they used it.

### 3.2.2 Sources of information

Sources of information for this study include:

➤ Personal observations and Interviews

From the society's experience and trend, the crops like carrot, beetroot, potato, onion, cabbage, and maize need 10,000 liters of water per day.

➤ Secondary data

Secondary data was obtained from international organizations like the FAO and different research papers.

### 3.2.3 Working Principles

The S-VAWT works because the pressures on each blade are different. The lower (concave) blade caught the wind and rotated the blade around its center vertical shaft. The upper blade (convex) collides with the blade, causing the air to be deflected sideways around it (Hadi Ali, 2013). When moving against the wind ( $F_{convex}$ ), the blades face less drag force due to their curvature than when moving with the wind ( $F_{concave}$ ). The Savonius turbine rotates due to differential drag, however, it cannot revolve faster than the wind speed. This indicates that the tip speed ratio is 1 or less.

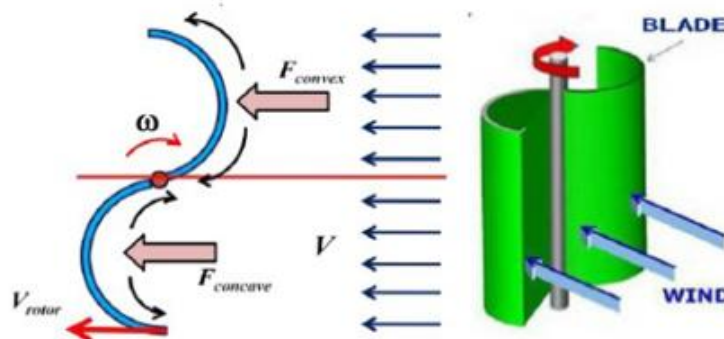


Figure 3. 2 Two bladed S-VAWT with the drag forces (Hadi Ali, 2013)

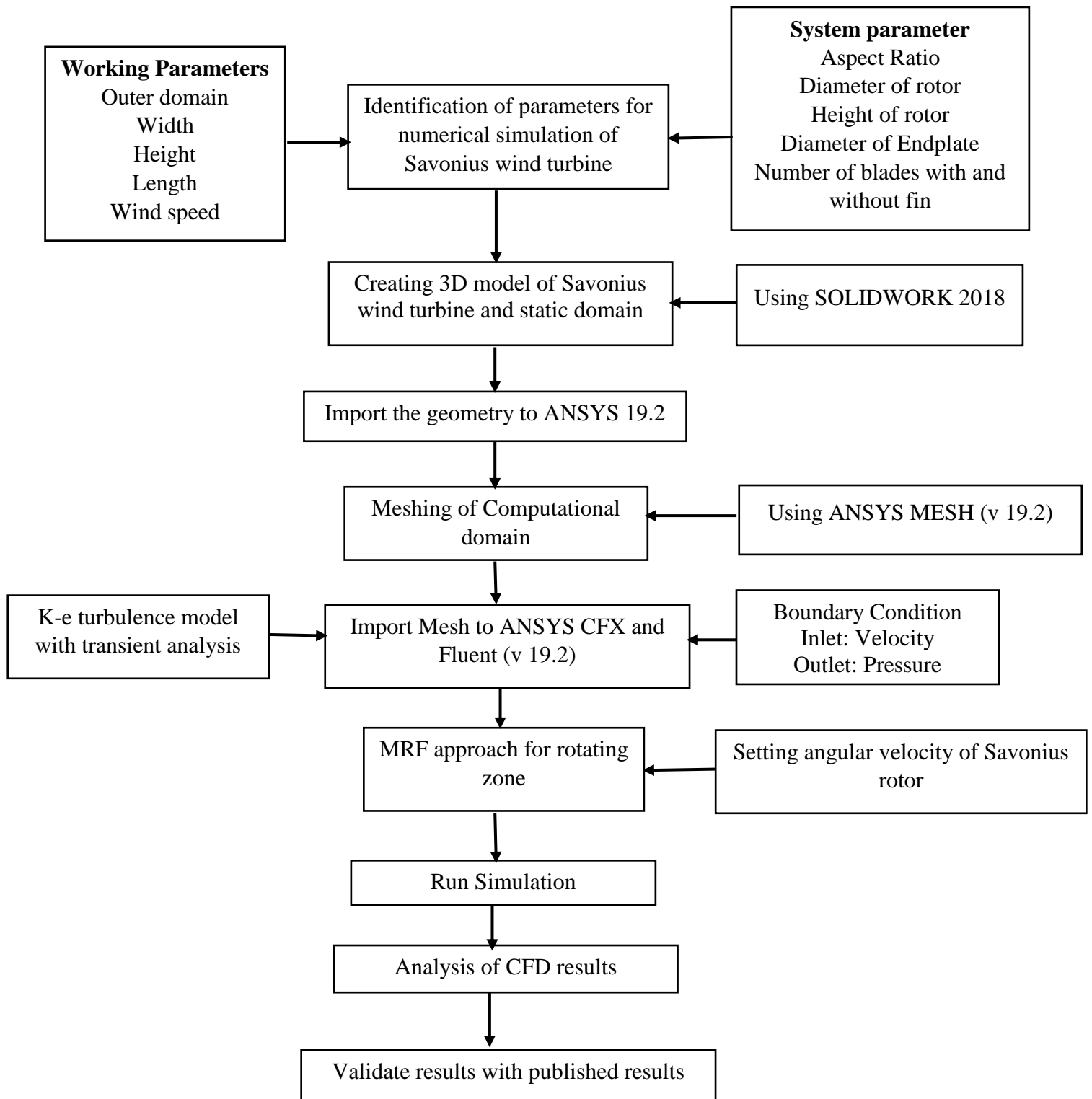


Figure 3.3 Flow charts of the methodology adopted for this study

### 3.3 Wind data

The required data is taken from the National Metrology Agency of Ethiopia (NMAE) for the selected area in recent 3 years. It includes 6 months (Dec.- May)

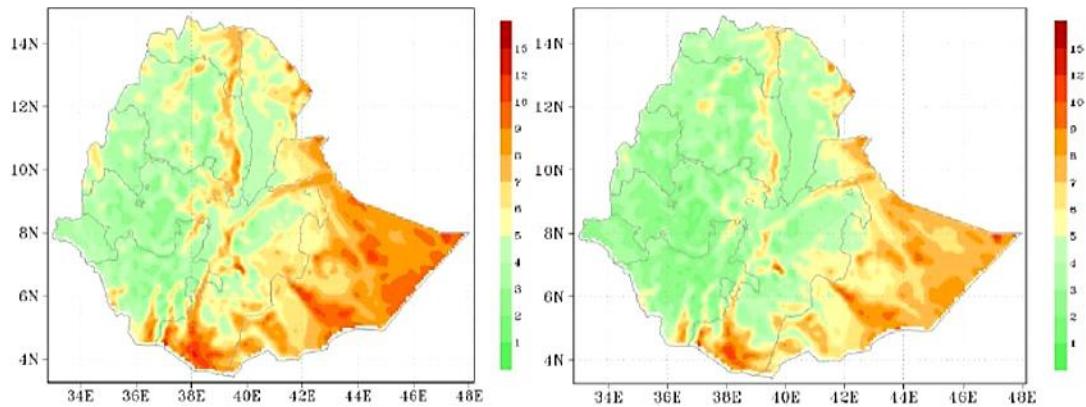


Figure 3.4 Distribution of average wind speed (m/s) in Ethiopia at heights of 50 m and 10 m respectively, from 2000 to 2009 (Misrak G. et al., 2015)

Table 3.1 Wind speed [National Metrology Agency of Ethiopia, NMAE]

Wind speed, V (m/s)									
Latitude	Longitude	Year, GC	January	February	March	April	May	December	Average
8.25	39.33	2015	2.3	2.3	2.4	2.5	1.5	2.6	2.27
		2016	2.3	2.5	2	1.5	1.4	2.4	2.02
		2017	2.4	2.5	1.9	2.3	1.8	2	2.15
Total average wind speed									2.15

Table 3.2 Monthly Temperature distribution  
(National Metrology Agency of Ethiopia, NMA)

Month	Temperature, °C								
	2015			2016			2017		
	Max.	Min.	Ave.	Max.	Min.	Ave.	Max.	Min.	Ave.
December	26.9	15.5	21.2	26.6	12.7	19.65	26	11.4	18.7
January	27	12.6	19.8	28.1	15.7	21.9	27.9	12	19.95
February	30.5	15.8	23.15	29.4	15.4	22.4	28.8	15.6	22.2
March	31.3	17.1	24.2	32.8	19	25.9	31.5	16.9	24.2
April	31.5	16.4	23.95	30.3	17.7	24	31.3	17.5	24.4
May	30.7	17.2	23.95	29.7	17.3	23.5	29.8	17	23.4
	Total ave.		22.71	Total ave.		22.89	Total ave.		22.14

Carrots, beets, potatoes, onions, cabbage, and maize are some of the crops that could be produced. 10,000 L of water per day is necessary for such crops, according to local experience and trends, and is available from a depth of 6-8 m underground.

Desing Input paramenters

Target location	Dodota
Available head, H	8 m
Required water flow rate, Q	10,000 L/day ( $1.1574 \times 10^{-4} \text{ m}^3/\text{s}$ )
Average ambient temperature, $T_a$	22.6°C
Avarage denisity of air $\rho_a$	1.136 kg/m <sup>3</sup>
Density of water $\rho_w$	996.5 kg/m <sup>3</sup>
Aspect ratio, AR	0.8

After having those data, the required power is calculated using the following steps.

***Required Water Power  $P_w$  and Pump power***

the required water power and the pump power can be determined using Equation 3.1 and 3.2 respectively.

$$P_w = \rho_w g Q H \quad (3.1)$$

$$P_p = \frac{P_w}{\eta_p} = \frac{\rho_w g Q H}{\eta_p} \quad (3.2)$$

where,

$\rho_w$	Density of water, kg/m <sup>3</sup>
$g$	Acceleration due to gravity, 9.81 m/s <sup>2</sup>
$Q$	Required Pump water flow rate m <sup>3</sup> /s
$H$	Available pump head, m
$\eta_p$	Pump efficiency

Taking the values required for equations 3.1 and 3.2 from the design parameters and the pump efficiency as 0.85, water power,  $P_w$  and pump power,  $P_p$  are determined to be **9.05 W** and **10.65 W** respectively.

List of equation to be used for the determination of mechanical power considering different losses are given as follows.

***Power On Pump Shaft,  $P_{SG}$***

$$P_{SG} = \frac{P_w}{\eta_{SG}} \quad (3.3)$$

***Power Transmitted from the Main Shaft to the Gearbox,  $P_{GB}$***

$$P_{GB} = \frac{P_{SG}}{\eta_{GB}} \quad (3.4)$$

***Power Input to the Main Shaft,  $P_{MS}$***

$$P_{MS} = \frac{P_{GB}}{\eta_{MS}} \quad (3.5)$$

***Power Expected from the Wind (Including Losses in the Rotor),  $P_r$***

$$P_r = \frac{P_{MS}}{\eta_r} \quad (3.6)$$

Where,

$\eta_{SG}$ ,  $\eta_{GB}$ ,  $\eta_{MS}$ ,  $\eta_r$  efficiency of pump shaft to the gear box (95%); efficiency of gear box (96%); efficiency of main shaft (95%) and efficiency of the rotor (96%) respectively.

Accordingly,  $P_{SG}$ ,  $P_{GB}$ ,  $P_{MS}$  and  $P_r$  are determined and their values are found to be 11.21 W, 11.68 W, 12.3 W and 12.81 W respectively.

The total power expected from the wind is determined considering all losses listed in tables 3.3 and 3.4

Table 3.3 Practical Efficiencies of various Mechanical devices (Burton *et al.*, 2011)

Factor	Efficiency
Rotor to the main shaft	92-97%
Main shaft to the gearbox	93-96%
Gearbox to the water pump	94-98%
Water (hydraulic) pump	80-90%

Table 3.4 Efficiency Comparison (Contents, no date)

Types of Gear	Efficiency
Spur	95-99 %
Worm	45-75 %
Helical	97-99 %
Bevel	96-99 %

***Power in the Wind,  $P_r$  and Power coefficient  $C_p$***

$$P_{\text{wind}} = \frac{P_r}{C_p} \quad \text{or} \quad C_p = \frac{P_r}{P_{\text{wind}}} \quad (3.7)$$

where,

$C_p$  Power coefficient

***Power coefficient,  $C_p$***

A wind turbine's power coefficient is the ratio of the maximum power generated by the wind to the total power available in the wind. The power that the Savonius rotor can harvest from the wind is primarily less than the real wind power available. The highest efficiency of a wind turbine that transforms wind power to the necessary is equivalent to  $\frac{16}{27}$  or 59 percent, according to Betz Limit. However, the practical value of  $C_p$  for various Savonius turbine designs ranges from 0.15 to 0.35 (Wenehenubun, Saputra, and Sutanto, 2015).



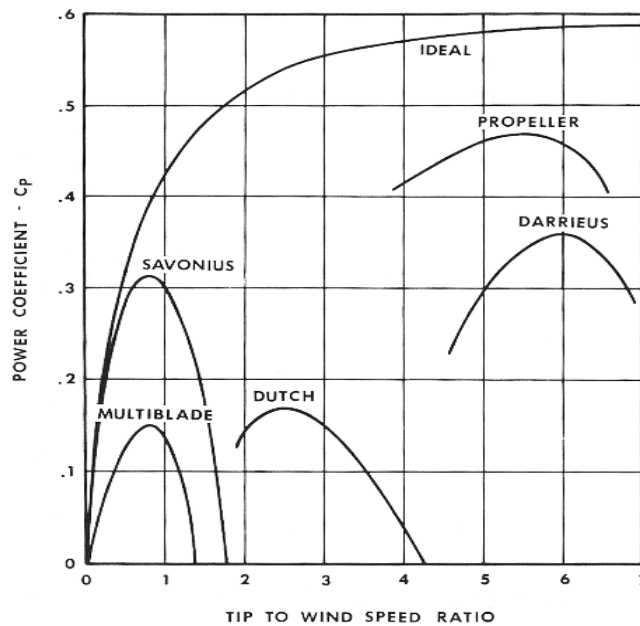


Figure 3.2 Curves of  $C_p-\lambda$  for different wind turbines (Wenhenubun, Saputra, and Sutanto, 2015)

From the graph, the maximum value of  $C_p$  for Savonius wind turbine is around 0.32. The power in the wind is then 40 W.

### 3.4 Aspect Ratio

Aspect ratio, AR, is defined as Aspect ratio,  $AR = \frac{H}{D}$  and is one of the parameters that affect the performance of the Savonius wind turbine. According to the majority of studies, the aspect ratio has an impact on Savonius wind turbine efficiency. When the aspect ratio, AR, is less than one, good outcomes are attained (Brusca, Lanzafame, and Messina, 2014).

$$AR = \frac{H}{D} \quad (3.8)$$

Where,

H rotor height, m

D rotor diameter, m

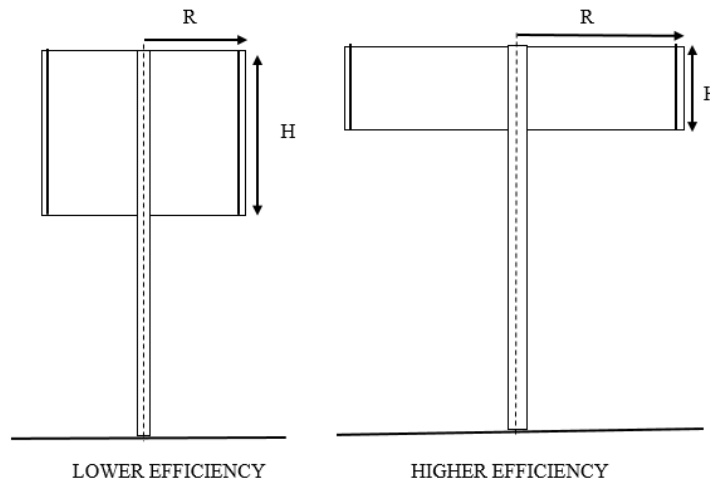


Figure 3.3 Savonius rotor with different Aspect Ratios (Brusca, Lanzafame and Messina, 2014)

### 3.5 Diameter of the rotor

Wind power is the time rate of change of the kinetic energy of the wind,  $d(KE)$  as given in Equation 3.9.

$$P_{\text{wind}} = \frac{d(KE)}{dt} = \frac{1}{2} V^2 \frac{dm_a}{dt} \quad (3.9)$$

This will give

$$P_{\text{wind}} = \frac{1}{2} \rho H D V^3 \quad (3.10)$$

where,

KE Kinetic energy of the wind,  $\frac{1}{2} m_a v^2$ , J

V velocity of air, m/s

From Equation 10 or Equation 7, the rotor diameter is determined to be **3 m**. Accordingly since the AR is 0.8, the rotor height will be 2.4 m.

The swept area is determined as follow by Equation 3.11.

$$A_s = H \times D \quad (3.11)$$

Hence, the swept area is 7.2 m<sup>2</sup>.

It the Diameter of endplate can be estimated to be 1.1 times the rotor diameter as recommended by (Anônimo, 1994)

$$D_e = 1.1D \quad (3.12)$$

### 3.5.1 Material selection

The material choice for the Savonius wind turbine rotors depends on many standards. Some of them are: (Eesof, Agilent, no date)

- ✓ Mechanical properties
- ✓ Availability
- ✓ Manufacturing consideration
- ✓ Cost
- ✓ Strength
- ✓ Rigidity

Because of its lightweight (cheap cost and noise reduction), corrosion resistance, stiffness, recyclable materials, strength at low temperatures, non-magnetic, and simple construction, aluminum is the best choice among many materials (Hadi Ali, 2013).

### 3.6 Number of blades

The rotor's rotation and the performance of wind turbine types are affected by the number of blades. According to many articles, the Savonius wind turbine with four blades has a greater power coefficient, good performance at a lower tip speed ratio, and high torque than those with two or three blades under the same test conditions. (Wenehenubun, Saputra and Sutanto, 2015). For this research, a4-blade conventional Savonius wind turbine is selected.

Some of the different types of blade shapes are: *semicircular*, *elliptical*, *conventional*, *helical* and *classical*.

### 3.7 Tip Speed Ratio, TSR ( $\lambda$ )

TSR,  $\lambda$  is the ratio between tangential speed from the rotor tip and the speed of the wind (Kurniawan, Dwi Prija Tjahjana and Santoso, 2020)

$$\lambda = \frac{V_r}{V} = \frac{\omega_r R}{V} \quad (3.13)$$

where,

$V_r$                                      $\omega R$ , tangential velocity of the rotor, m/s

$\omega_r$                                     angular velocity of the rotor, rad/s

R radius of the rotor, m

The value of  $\lambda$  is referred from the graph as 0.7, (Brusca, Lanzafame and Messina, 2014). Hence the angular velocity,  $\omega_r$ , is determined to be 1.003 rad/s

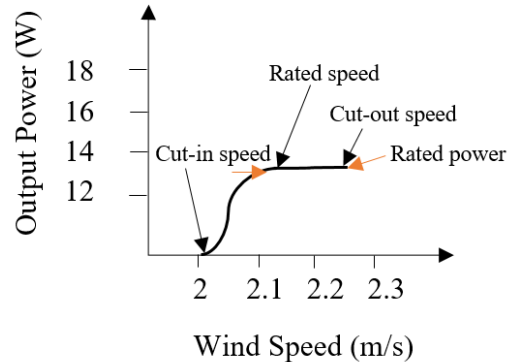


Figure 3. 4 Power curve graph

### 3.8 Selection of Pump

A pump is a mechanical device that uses to transfer fluid by converting the fluid's mechanical energy into pressure energy(hydraulic energy) orit is a hydraulic device that lifts fluids from low to high levels and moves fluids from low to high-pressure areas.

The selection of pump depends upon

- ✓ The type of fluid desired to pump,
- ✓ The distance desired to move the fluid,
- ✓ The quantity required to get over a particular period.
- ✓ Availability and cost

For this system, a Radial flow centrifugal pump is considered since it is mostly applicable for low flow rate and high-pressure applications.

## CHAPTER FOUR

### MODELLING AND NUMERICAL ANALYSIS

#### 4.1 Geometry and Computational Domain

The 3D geometry was created in SOLIDWORK 2018 with the settings specified below and then imported to ANSYS 19.2. From the creation of a 3D CFD model, mesh generation, and setting of the CFX solver to results analysis in CFD-Post, ANSYS Workbench provides a framework for developing a workflow. To solve the Navier- Stokes equations and capture the continuous change in flow field due to turbine rotation, the CFX solver employs unsteady Reynolds-Averaged Navier-Stokes (URANS) in conjunction with the  $k-\epsilon$  turbulence model. Computational fluid dynamics is a valuable design tool that can execute, evaluate, and optimize a large number of simulations for wind power study. The velocity and pressure on the rotor can be predicted using CFD computations. These can then be used to predict the turbine's power coefficient.

Table 4. 1 Design parameter for the Savonius wind turbine

No.	Parameter	Values
1	Rotor diameter, D	3m
2	Rotor height, H	2.4 m
3	Swept Area, $A_s$	7.2 m <sup>2</sup>
4	Blade diameter, d	1.5 m
4	Number of blades	4
5	Blade thickness	2 mm
6	Shaft diameter, $d_s$	20 mm
7	Endplate diameter, $D_e$	3.3 m
8	Tip Speed Ratio, TSR	0.7
9	Aspect ratio, AR	0.8

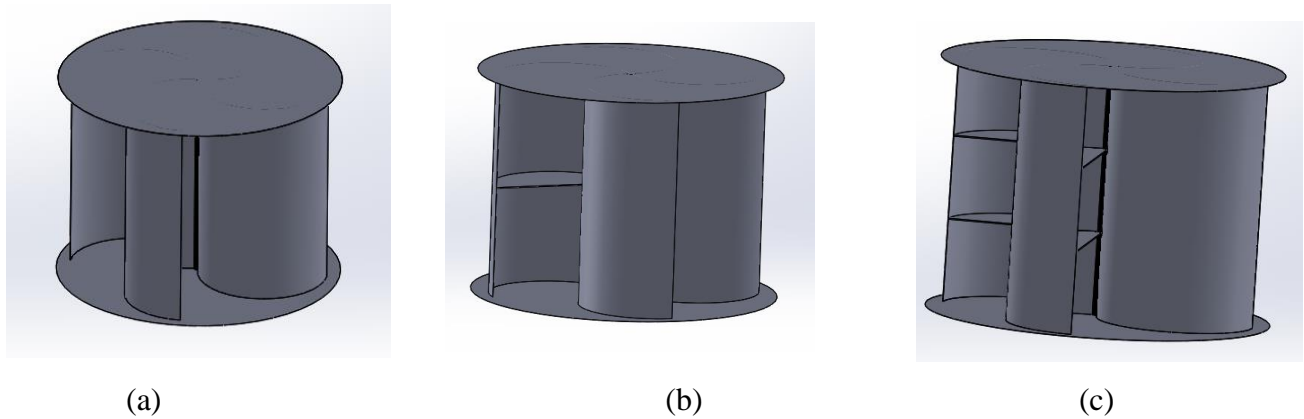


Figure 4. 1 Savonius blades (a) without fin (b) with 1 fin (c) with 2 fin

The maximum number of added fins to the blade's rotor is two. As the number of added fins increase, the turbine will not rotate at the required speed because, the force in the concave side is lower than convex side, due to the friction force between the fins and the blades.

The entire computational domain resembles a rotor immersed in an open channel (stationary zone), as illustrated in the following diagram, where the Z-axis is the turbine's rotation axis.

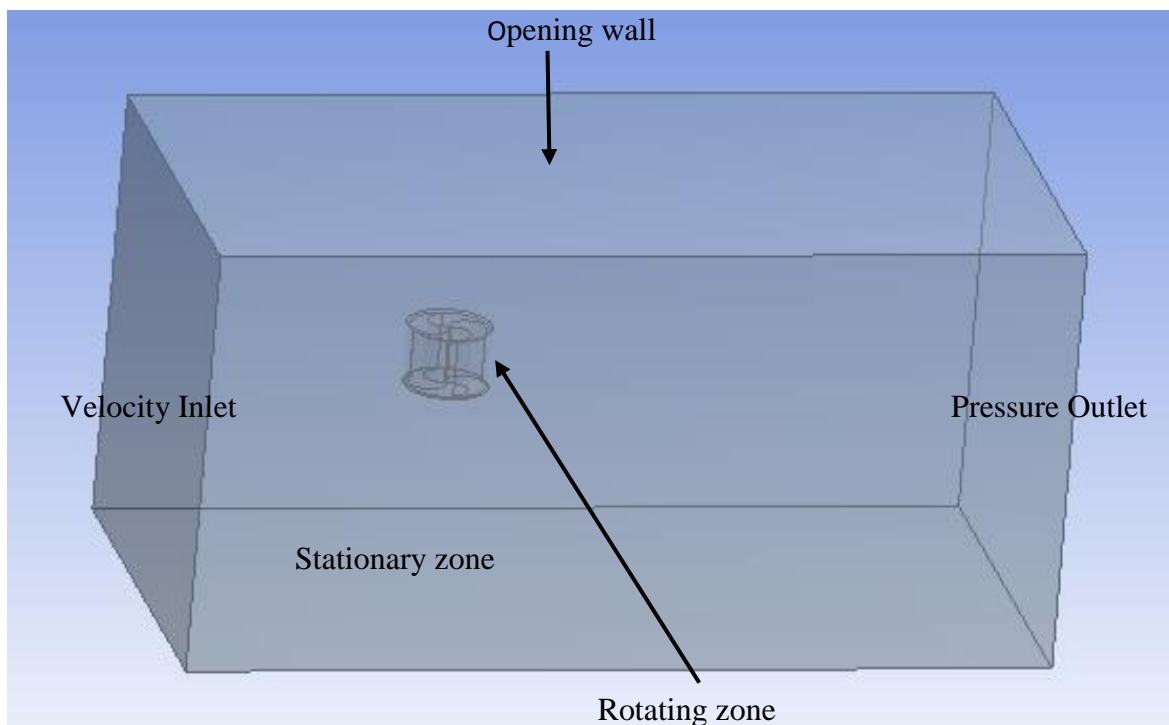


Figure 4. 2 Computational domain immersed Savonius rotor in open channel

The domain used in the savonius wind turbine modeling is divided into two parts (Pujari *et al.*, 2021)

➤ Inner (rotating) domain

It consists of wind turbines and fluids that are impacted by rotating turbine conditions, and it is 1.75 times the diameter of the rotor.

➤ Outer (static) domain

It has a constant wind condition and is a rectangle in shape, with a length of  $12D$ , a depth of  $3D$ , and a height of  $6D$ , where  $D$  is the rotor's diameter. Those dimensions must be large enough to eliminate the impacts of walls (Pujari *et al.*, 2021). Also, it is known as an open channel.

The turbine with  $0^\circ$  blade orientations is positioned inside the outer domain, which is programmed as a moving mesh, while the outer domain is large enough to avoid the effects of the walls. The domain size for this study is  $36\text{ m} \times 9\text{ m} \times 18\text{ m}$ , with a rotating domain size of  $5.25\text{ m}$ .

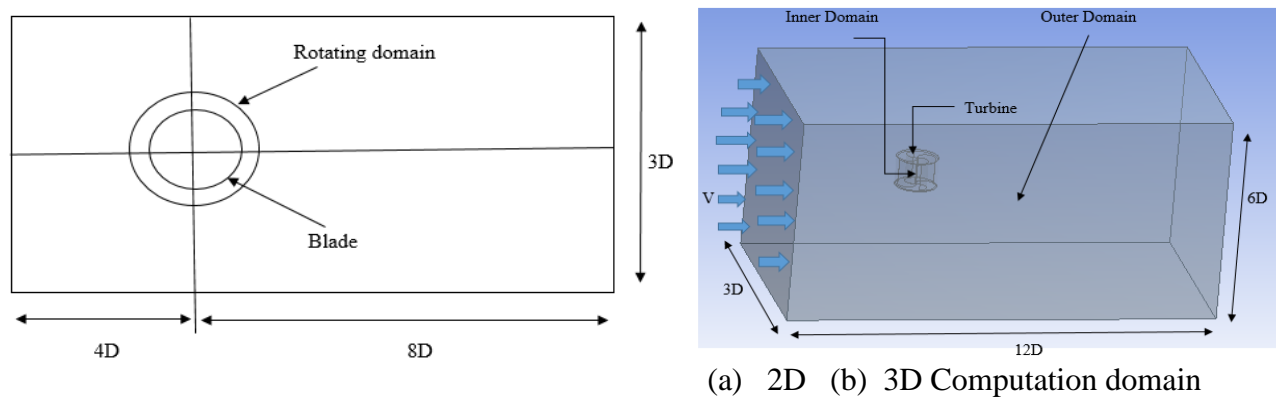


Figure 4. 3 Savonius wind turbine modeling domain

The table below shows the boundary conditions used for numerical analysis, and the same is shown in Fig. below. During the CFD study, the left side of the channel has been set as a velocity inlet, where air enters through space at free stream velocity.

The uniform velocity distribution of  $2.15 \text{ m/s}$  is set according to the rated design specifications at the inlet of the computation zone. The extreme right boundary in the same direction was set as an outflow condition, with a standard atmospheric pressure provided and a no-slip wall applied to the blade's boundary wall. Symmetry is given to the channel's top. Free surface effects are not considered in this simulation since it is assumed that the turbine works at the right depth to minimize the surface effect. The Savonius turbine inside the rotating zone has a rotating wall condition (no-slip wall).

Table 4. 2 Boundary conditions for numerical analysis

Name	Boundary type	Boundary Condition
Inlet	Velocity Inlet	$2.15 \text{ m/s}$ , uniform flow
Outlet	Pressure Outlet	Outflow, 1 atm (standard atmospheric pressure)
Sides of the outer domain	Free slip wall	Stationary
Top and bottom walls of the outer domain	Symmetry	Symmetry
Savonius Turbine	No-slip wall	Rotates at a desired angular velocity

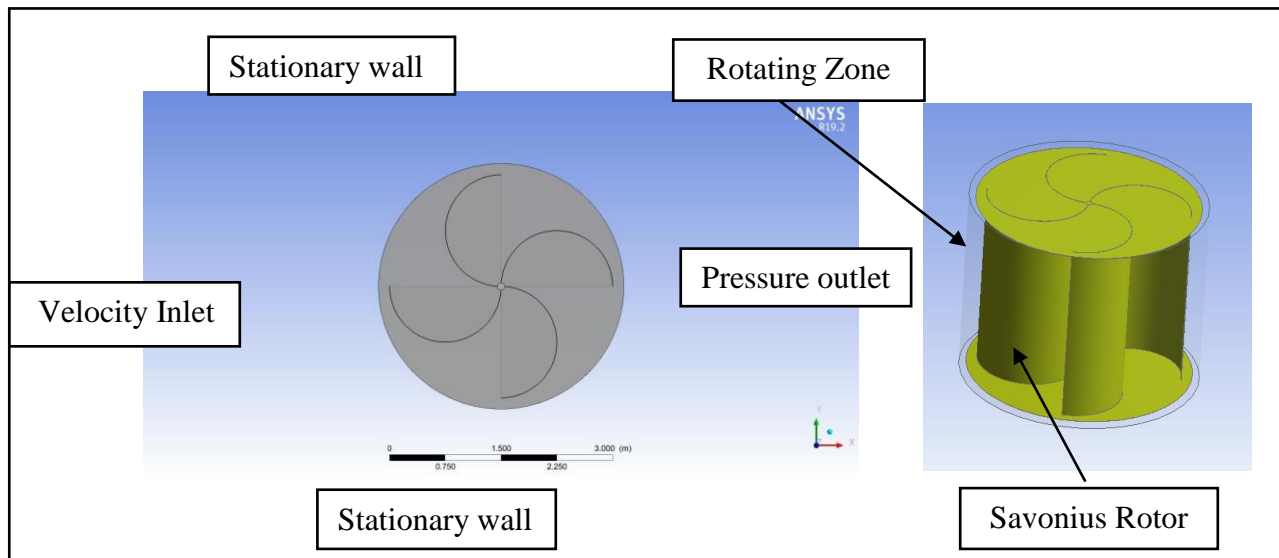


Figure 4. 4 Boundary Conditions for CFD analysis



#### 4.2 Modeling of the Savonius Wind Turbine

The entire computational domain is imported to ANSYS MESH to develop the mesh. Tetrahedral mesh is used in the meshing process for simulating S-type savonius wind turbines because it can mesh complex geometry for each computational subdomain. Sizing is used in the modeling domain, as seen in the table below. The smooth setting category includes the sizing utilized in this investigation. The goal of scaling is to have a more realistic simulation result as well as a smoother visual aspect.

The precision of the simulation findings is significantly influenced by the amount of division used in this sizing. Because this is a CFD analysis and the contact regions are not automatically resolved, two interface zones are created by naming the outside surface of the inner fluid zone (Interface-Inner) and the in-contact surface of the outer fluid zones interface-outer.

Table 4.3 Sizing Model

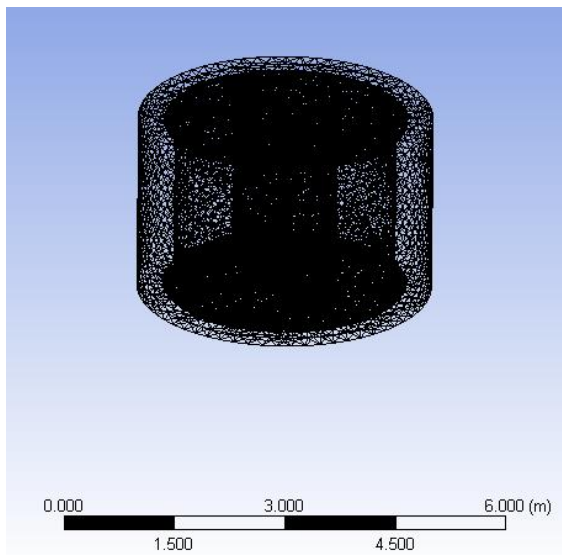
Sizing	
Resolution	7
Smoothing	High
Transition	Slow
Span angle center	Fine
	Medium
	Course

The table below shows the several aspects of mesh quality generated for each subdomain, all of which are found to be within acceptable limits (Kumar and Saini, 2017).

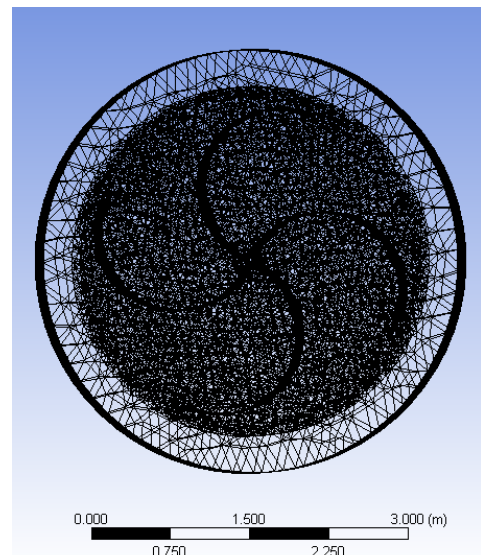
Table 4. 4 Mesh qualities of the study

Quality aspect	Rotating zone			Stationary zone		
	Course	Medium	Fine	Course	Medium	Fine
Number of elements	311584	301597	352732	1179159	1179159	1179159
Number of Nodes	438571	425169	498730	1637131	1637131	1637131
Skewness (Av.)	0.33946	0.34102	0.31485	0.21188	0.21188	0.21188
Orthogonal quality (Av.)	0.65937	0.65779	0.68396	0.78677	0.78677	0.78677

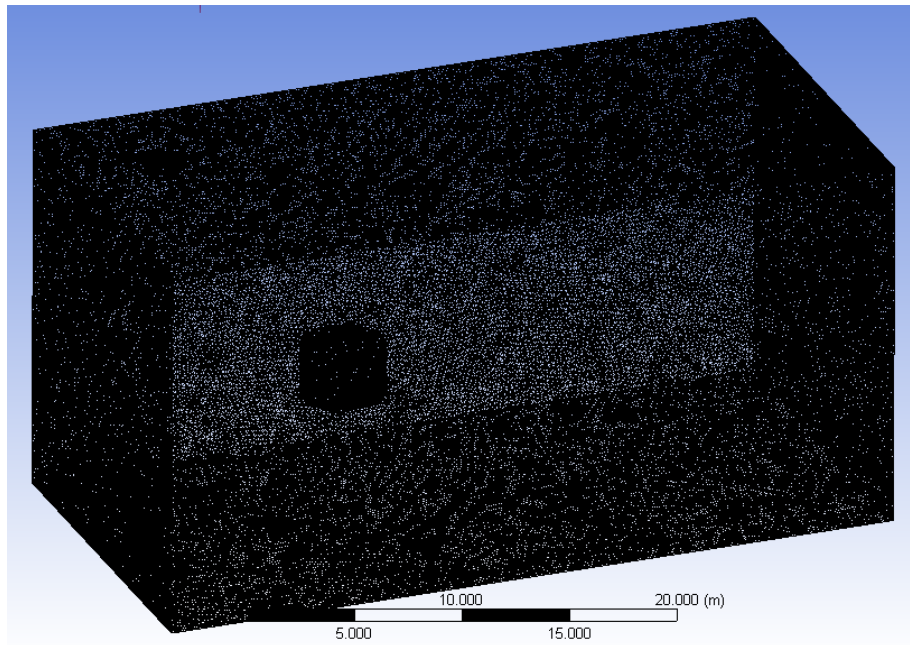
In this simulation, the meshing results are displayed in the Figure below.



(a) Computational domain around the blade



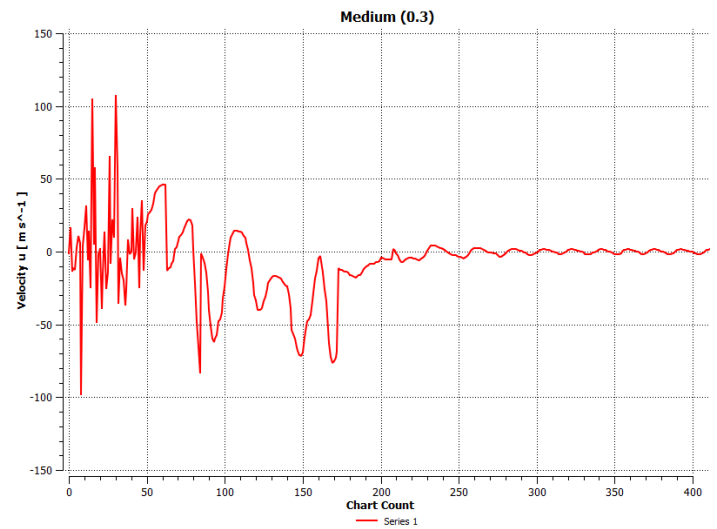
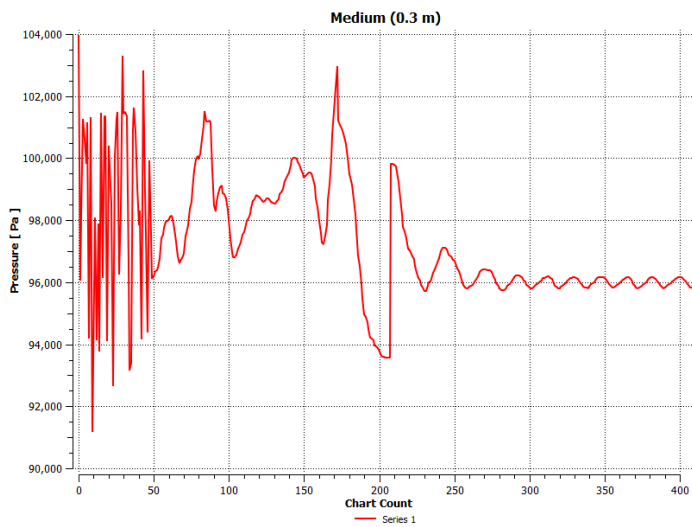
(b) Top view



(c) Computational grid of both domains

Figure 4.5 Meshing results of Savonius wind turbine

Element size for all span angle center is taken as 0.3 m. To select the mesh size, mesh independency test must be check for all span angle center and their graph is displayed as follows.



# Performance Analysis and Simulation of Savonius Wind Turbine for Small-Scale Water Pumping System

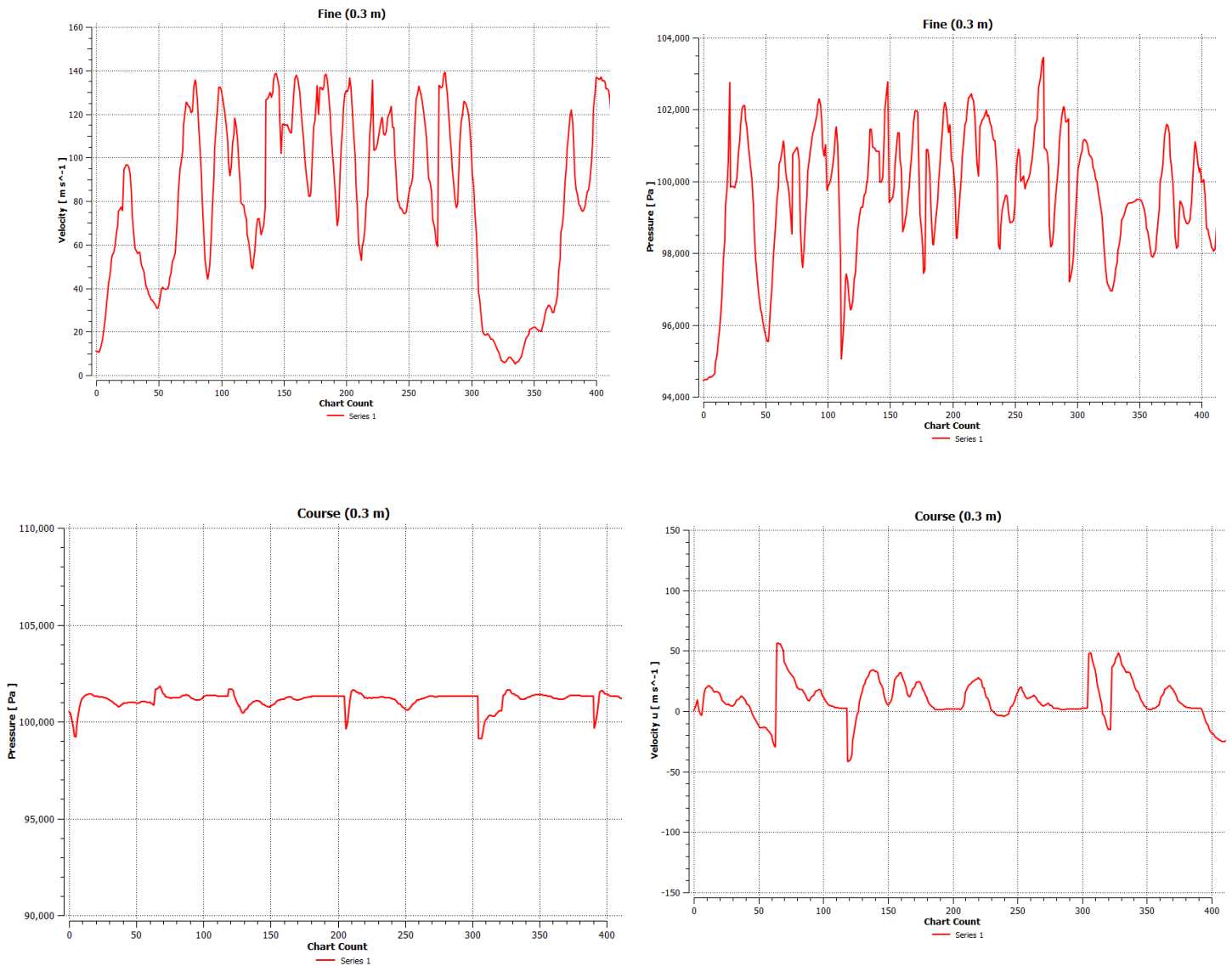


Figure 4. 6 Mesh independency graphs for medium, fine and course span angle center respectively

For all cases pressure and velocity graph is checked for mesh independency. From the graph result, fine span angle center with sizes of 0.3 m is selected and suitable for this case.

### 4.3 Simulation Procedure

The developed mesh on the geometry is exported to the ANSYS CFD computational solver, which defines and solves the relevant boundary conditions. Unsteady Reynolds Averaged Navier- Stokes equations are solved using the finite volume approach to explain the flow field.

#### 4.3.1 Turbulence model

Without resolving all scales of the smallest turbulent variations, turbulence models are used to predict the effects of turbulence in fluid flow. The SST k-model, standard k-turbulence model, Realizable k-turbulence model, and RNG k-turbulence model have all been employed in previous studies (Kumar and Saini, 2017). The standard k-  $\epsilon$  turbulence model is used, which solves two separate transport equations and allows the turbulent kinetic energy (k) and its dissipation rate to be determined independently ( $\epsilon$ ). The standard k-  $\epsilon$  turbulence model is excellent for determining fluid flow problems in the vicinity of complex geometries, as well as the accuracy of results over a vast turbulence flow area (Saputro *et al.*, 2021).

The transport equations for k and  $\epsilon$  in the Standard k- $\epsilon$  model are given as (Canonsburg, 2018).

$$\frac{\partial(\rho k)}{\partial t} + \frac{\partial}{\partial x_j} (\rho U_j k) = \frac{\partial}{\partial x_j} \left[ \left( \mu + \frac{\mu_t}{\sigma_k} \right) \frac{\partial k}{\partial x_j} \right] + P_k - \rho \epsilon + P_{kb} \quad (4.1)$$

$$\frac{\partial(\rho \epsilon)}{\partial t} + \frac{\partial}{\partial x_j} (\rho U_j \epsilon) = \frac{\partial}{\partial x_j} \left[ \left( \mu + \frac{\mu_t}{\sigma_\epsilon} \right) \frac{\partial \epsilon}{\partial x_j} \right] + \frac{\epsilon}{k} (C_{\epsilon 1} P_k - C_{\epsilon 2} \rho \epsilon + C_{\epsilon 1} P_{\epsilon b}) \quad (4.2)$$

where,

$C_{\epsilon 1}, C_{\epsilon 2}$                       k-  $\epsilon$  turbulence model constant, 1.44 and 1.92 respectively

$\sigma_k, \sigma_\epsilon$                         k-  $\epsilon$  turbulence model constant, 1 and 1.3 respectively

k                                      turbulent kinetic energy

$U_j$                                     velocity components

$\rho$                                       density of the fluid

$\epsilon$                                       dissipation rate of the turbulent kinetic energy

t                                        time

$x_j$                                     Cartesian coordinate

$\mu, \mu_t$  viscosity and turbulent viscosity respectively

$P_k$  is the turbulence production due to viscous forces, and modeled using:

$$P_k = \mu_t \left( \frac{\partial U_i}{\partial x_j} + \frac{\partial U_j}{\partial x_i} \right) \frac{\partial U_i}{\partial x_j} - \frac{2}{3} \frac{\partial U_k}{\partial x_k} \left( 3\mu_t \frac{\partial U_k}{\partial x_k} + \rho k \right) \quad (4.3)$$

$P_{kb}$  and  $P_{\epsilon b}$  represent the influence of the buoyancy forces, and assumed to be proportional, and positive.

$$P_{kb} = -\frac{\mu_t}{\rho \sigma_\rho} g_i \frac{\partial \rho}{\partial x_j} \quad (4.4)$$

$$P_{\epsilon b} = C_3 \cdot \max(0, P_{kb}) \quad (4.5)$$

Boundary conditions are implemented after establishing an acceptable turbulence model, as previously mentioned. The performance of a Savonius rotor and the quality of fluid flow around it may be affected by turbulent conditions. The turbulence quantities like turbulence intensity and turbulent viscosity ratio should be supplied at the boundary where inflow occurs (Kumar and Saini, 2017). Turbulence intensities of less than 1% are regarded as low, while those of more than 10% is considered strong. Kumar & Saini, 2017 also found that as the turbulence intensity in the fluid flow increases, the maximum averaged power coefficient drops. As a result, the turbulence intensity is set to 5%, whereas the turbulent viscosity ratio is set at 10% at the inlet and outlet boundary conditions.

The simulation is carried out using a pressure-based solver with an absolute velocity formulation. The blades rotate at an angular velocity determined by the tip speed ratio, while the outer domain remains stationary. This rotating region is solved by modified Navier-Stokes equations. The rotating zone is set to an angular velocity of the Savonius turbine using the Frozen Rotor-Stator approach.

An interface connects the Savonius turbine's rotation, the rotating zone, and the stationary zone (open channel) to the model. To get a solution and assure the stability of the calculations, all simulations are performed in an unstable or transient state condition. To perform the simulations, a pressure–velocity coupled solver called the Semi-Implicit Method for Pressure-Linked Equations is used.

For the spatial discretization of all convection terms, such as the equation of momentum, turbulent kinetic energy, and turbulent dissipation rate, a Second Order Upwind Scheme is used. Second-order techniques can help eliminate interpolation inaccuracies and false numerical diffusion. A First Order Implicit Formulation is used for the transient algorithm. To achieve convergence, monitor for residuals of an iterative process for momentum, and turbulence equations are fixed equal to  $1 \times 10^{-4}$ . The order of all residuals magnitudes reduced below a value of  $1 \times 10^{-4}$  for each time step, showing simulation process convergence.

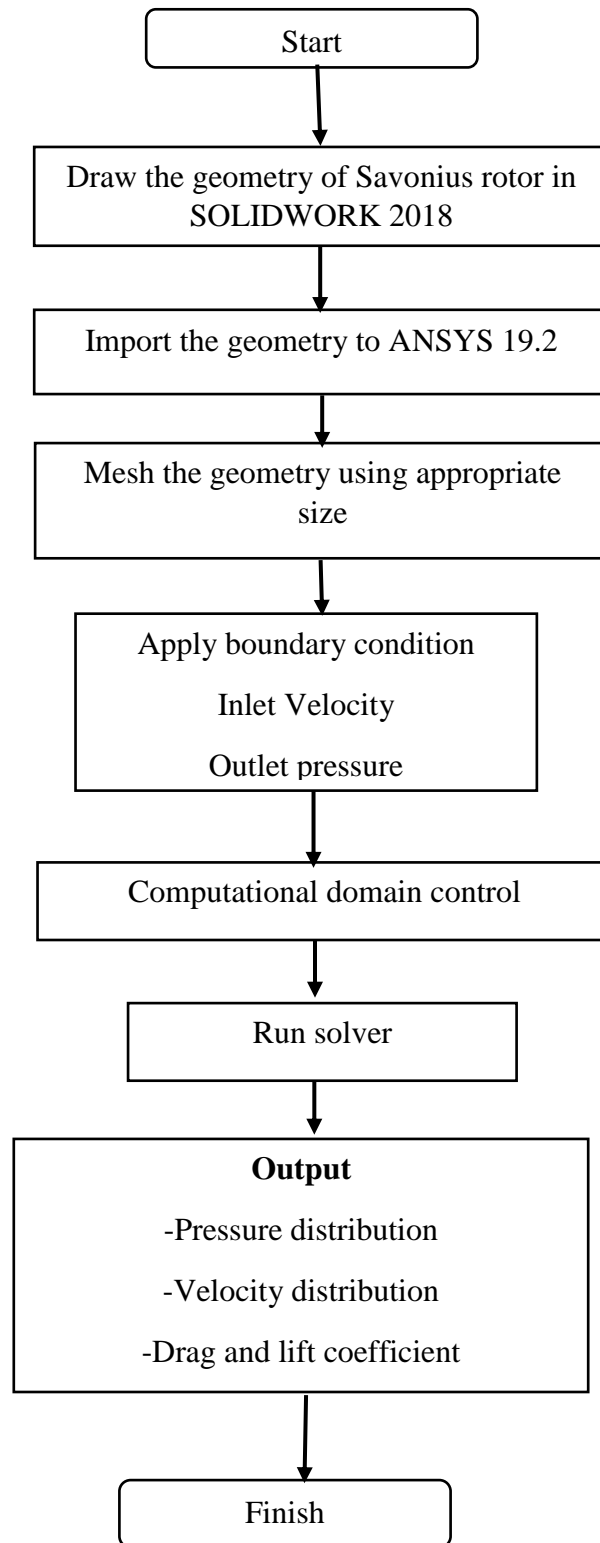


Figure 4. 7 Flowchart Simulation



## CHAPTER FIVE

### RESULT AND DISCUSSION

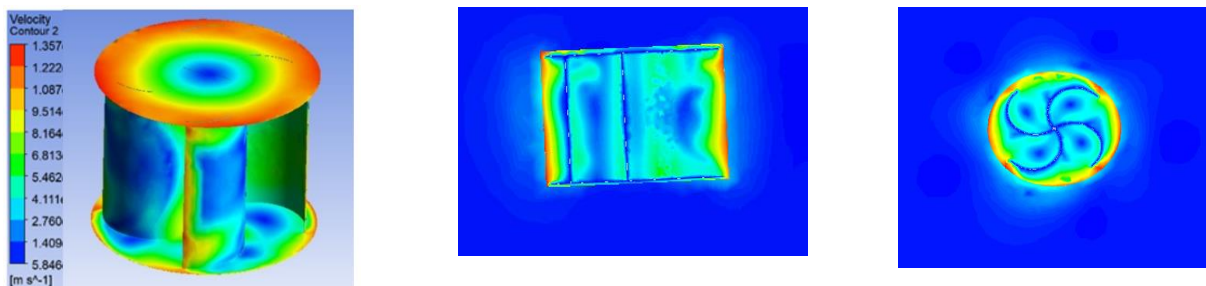
This chapter includes a graphical representation of the velocity and pressure distributions, numerical output for evaluating design parameters, and validation of the CFX result versus previously published data.

#### 5.1 Graphical Displays

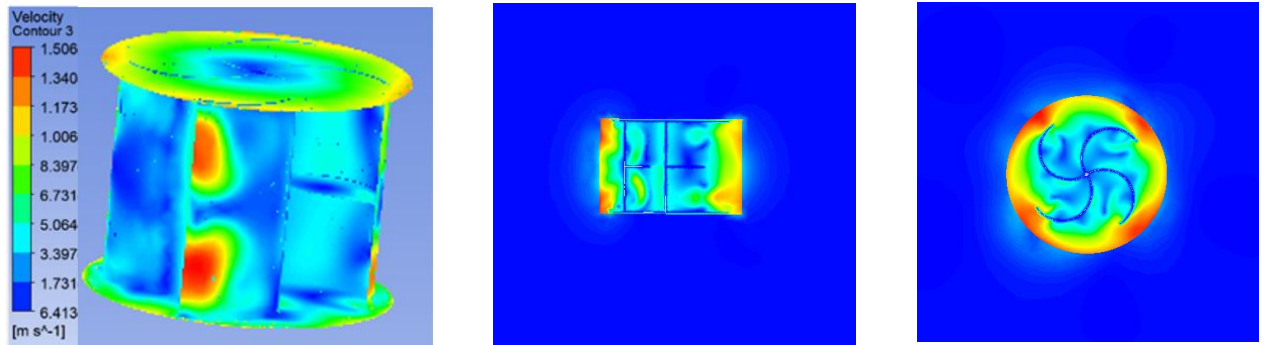
The numerical output, graphical display, various forms of charts, and animation are all examples of CFD post-analysis output forms. Among these, a graphical display is employed in this part to discuss the flow domain's output result. The graphical display option is used to see the overall flow pattern in the Savonius rotor flow domain. With conventional  $k-\epsilon$ , some graphical displays are used to show the velocity and pressure distributions of the rotor with one fin, two fins, and without a fin.

##### 5.1.1 Velocity distribution

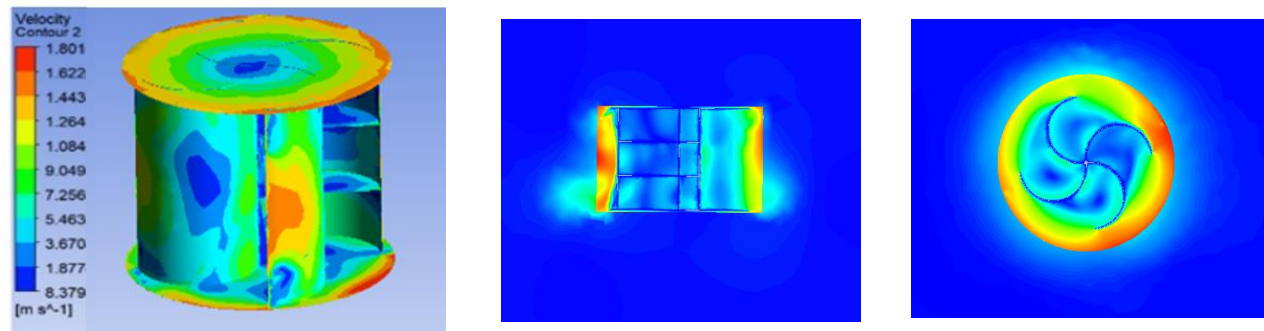
The variations in velocity near the blades in the flow domain are predicted using velocity contours plots. The highest wind speed or velocity distribution of  $1.801 \text{ m/s}$  can be seen in the dispersion of wind speed in the savonius with two fins. At the top and bottom of the turbine, as well as at the tip of the blade, this wind speed can be seen hitting the sidewalls of the endplate. The darker blue color also shows that the wind speed entering the turbine area is steadily decreasing. The maximum wind speed or velocity distribution values for one and no fin additions are  $1.506 \text{ m/s}$  and  $1.357 \text{ m/s}$  respectively.



(a)



(b)



(c)

Figure 5. 1 Velocity distribution for (a) without fin (b) 1 fin (c) 2 fins

The velocity contours of a Savonius turbine with a  $0^\circ$  twist angle and a tip speed ratio of 0.7 are compared to the results of a study conducted by (Ridwan, Setyawan and Setiyono, 2019). A comparison is done to validate the velocity pattern around the rotor to show the similarities in the results. The velocity pattern at the inlet is determined to meet the provided boundary condition.

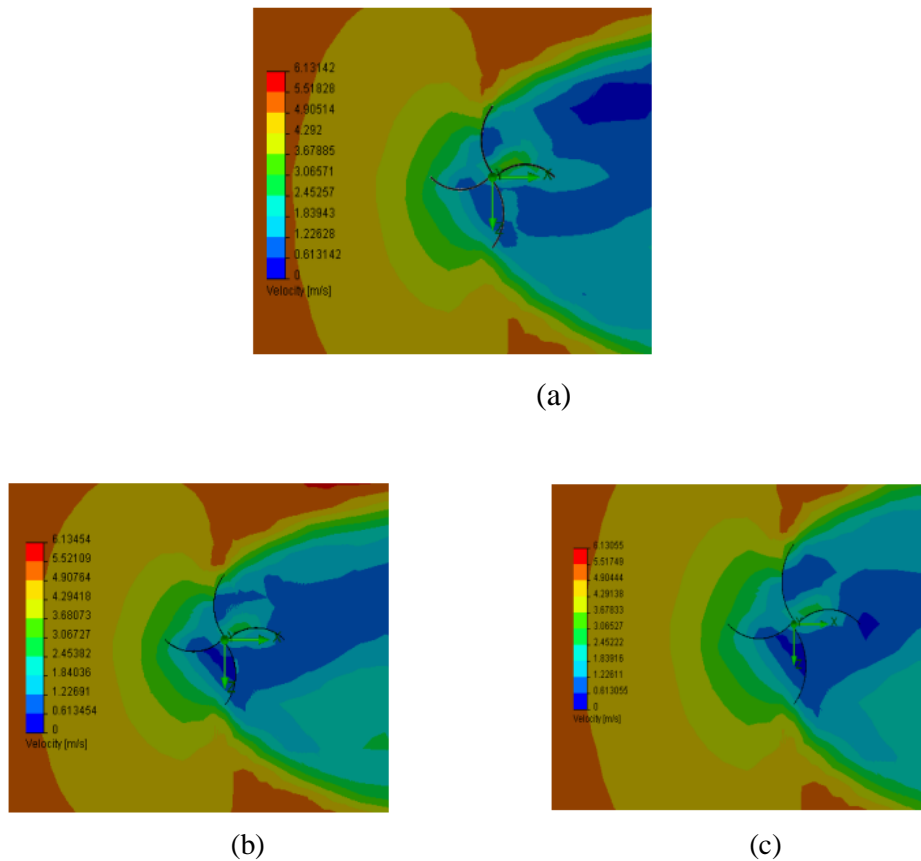


Figure 5. 2 Velocity distribution done by (Ridwan, Setyawan and Setiyono, 2019) (a) without fin (b) 1 fin (c) 2 fins

Velocity streamlines are lines that are drawn tangential to the velocity vector at each place in the flow at a given instant. Velocity Streamlines help in the understanding of rotor flow. The magnitude of velocity is represented by the color of the vector, while the vector direction represents the flow direction. Velocity streamlines are monitored to study the entire flow profile around the Savonius rotor.

The fluid velocity is zero at the stagnation point, and all kinetic energy has been transformed to pressure energy. After passing through the Savonius rotor, the pressure begins to rise again, and the flow experiences an opposing pressure gradient. The flow separates from the surface due to the negative pressure gradient, resulting in a very turbulent zone surrounding the rotor. The awake zone emerges in the flow domain around the rotating Savonius rotor due to flow separation and

recirculating flow. As the flow separates, the pressure inside the wake zone remains low, resulting in a net pressure force (pressure drag).

The addition of fins on the blade turbine guides the wind flow to fill the space in the blade more quickly, according to the velocity streamline. The blade will rotate at a slower speed with the added fin than without it. Because of the smaller area created by the addition of a fin, pressure along the turbine is raised. Both sides of the turbine area will experience increased pressure. Because both turbine sections have reached higher pressure, the pressure difference between the two blades will be reduced. The positive drag force on the blade will be reduced as the pressure difference decreases.

### 5.1.2 Pressure distribution

Pressure drops across the rotor from the upstream to the downstream side, as seen in the diagrams below. Pressure is uniform at the inlet, but larger pressure values are seen upstream, on the concave side of the advancing blade and the convex side of the returning blade. On the downstream side, a lower pressure zone develops (the convex side of the advancing blade and the concave side of returning blade). Within the flow domain, two pressure areas, greater and lower, are present near the blades, resulting in a pressure drop. The pressure drop across the rotor causes the turbine blades to rotate, causing the Savonius turbine to extract power from the flowing wind speed. Without fin addition, the pressure distribution shows maximum pressure ranges of 101.7 kPa -106.4 kPa and a minimum pressure of 83.04 kPa. The pressure is highest on the blade's inner side and progressively reduces on the outside. The pressure difference is 23.36 kPa.



Figure 5.3 Pressure distribution of Savonius rotor without fin

The pressure on the turbine blade shows a maximum value of 108.5 kPa in the figure below of pressure distribution with one fin. In this variation, the blade's inner pressure is also higher than the outer pressure. It is in the range of 104.3 kPa – 108.5 kPa in the concave area characterized by high pressure, and 87.54 kPa in the convex area dominated by low pressure. The highest pressure value with two fins is 112.2 kPa. It is between 106.0 and 112.2 kPa in the concave area, and 84.35 kPa in the convex section. The pressure difference for blades with 1 fin and 2 fins are 20.96 kPa and 27.85 kPa respectively.

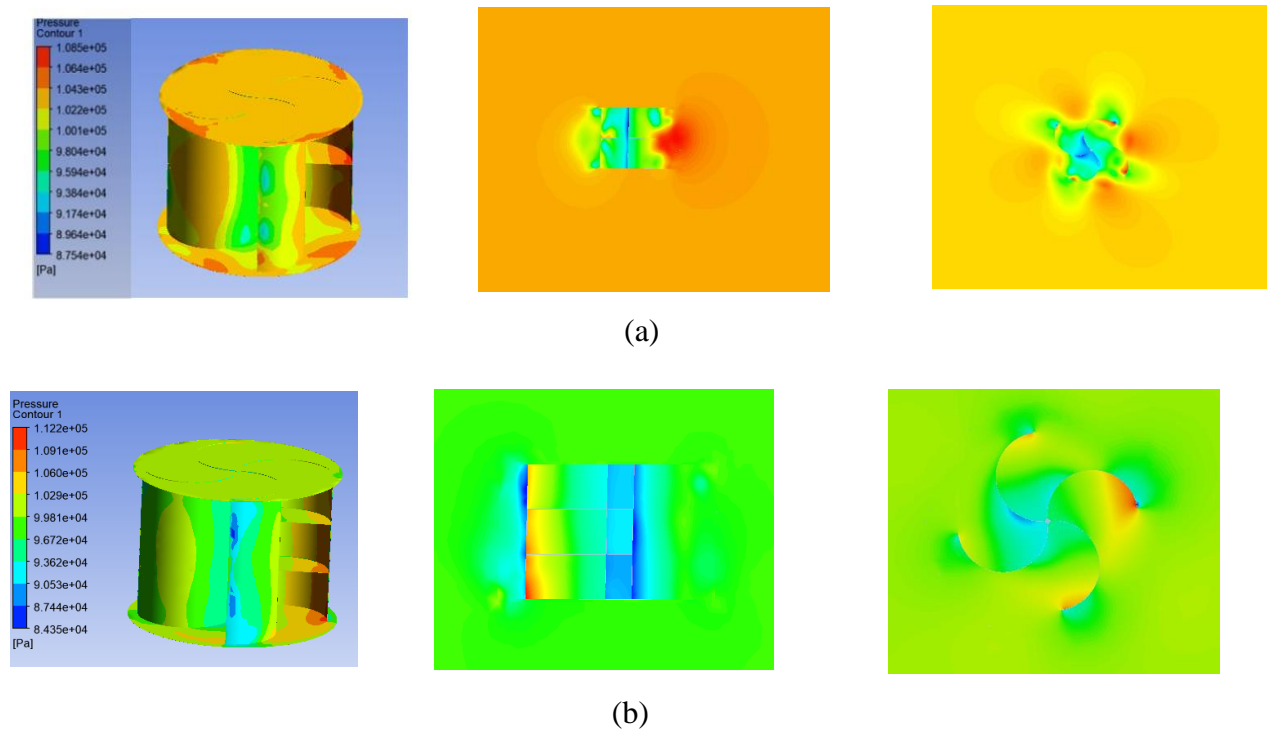


Figure 5. 4 Pressure distribution (a) with one fin (b) with two fins

The results of a study conducted by (Ridwan, Setyawan and Setiyono, 2019) are compared to the pressure contours of a Savonius turbine at  $0^\circ$  twist angle at  $TSR=0.7$  for the corresponding velocity. A comparison is done to validate the velocity pattern around the rotor and the pattern of velocity at the inlet is found to be similar for the specified boundary condition to show the similarities in the results. The highest pressure for the conventional blade without the fin is 101.343 kPa and the smallest pressure is 101.311 kPa, as shown in Figure (a). (b) The highest pressure

is 101.340 kPa, while the smallest Pressure is 101.310 kPa for the conventional-type blade with one fin. The conventional-type blade with two fins figure (c) has a maximum pressure of 101.344 kPa and a minimum pressure of 101.310 kPa. With the addition of a fin, the area of pressure increases, with a blade with two fins having the biggest area at 101.344 Pa.

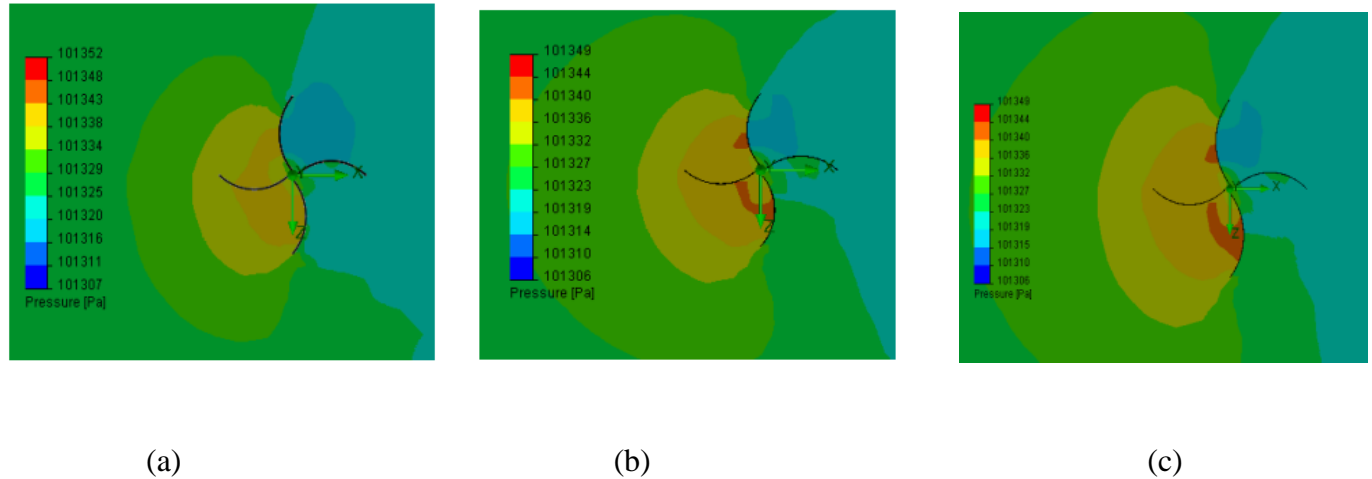


Figure 5. 5 Cut plot pressure by (Ridwan, Setyawan and Setiyono, 2019) (a) without fin (b) 1 fin (c) 2 fins

## 5.2 Effect of Aspect Ratio, AR

For this study, the aspect ratio is 0.8 and it results coefficient of performance,  $C_p$  0.28. this result is better when compared to Kumar & Saini, 2017 results which is  $C_p$  0.23 for the aspect ratio of 1. This shows, as the aspect ratio,  $AR = \frac{H}{D}$ , increases (the diameter of the rotor blade decreases), the performance power coefficient,  $C_p$ , gets smaller.

## 5.3 Effect of adding fins to the savonius rotor on the power coefficient

The power coefficient indicates how much wind energy can be produced from wind kinetic energy through the turbine rotor cross-section. The value of the power coefficient without fins and with fins at a wind speed of  $2.15 \frac{m}{s}$  is presented in Fig. below, based on the CFD ANSYS 19.2 simulation. The graph showed that the  $C_p$  value in the Savonius turbine with two fins increases at an average of 0.0184 for each 0.1 increase in tip speed ratio, while the  $C_p$  value in the Savonius turbine without a fin and with one fin increases at an average of 0.0083 and 0.01 for each additional 0.1 tip speed ratio, respectively. These results indicate that the savonius wind turbine with the

addition of 2 fins is better with a maximum power coefficient of 0.256 than without a fin and 1 fin.

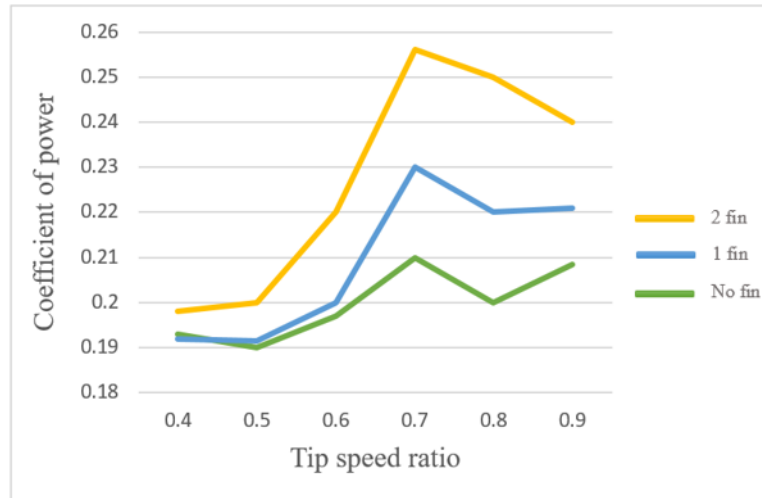


Figure 5. 6 Comparison of power coefficient for blades without a fin, 1 fin, and 2 fins addition

#### 5.4 Comparative analysis of Drag and Lift Coefficient

A positive drag force is used in the Savonius wind turbine. The operational Reynolds number has a significant impact on drag characteristics (flow velocity). The power coefficient of a vertical-axis wind turbine is strongly influenced by the Reynolds number. With increasing Reynolds number, the maximum coefficient of power increases. Furthermore, the Reynolds number of the blade changes as the major parameters of the turbine rotor change, i.e. as the rotor diameter increases, the Reynolds number of the blade increases. According to the result from Fluent Ansys for lift and drag coefficient, the addition of a fin increases the drag coefficient. Finally, adding two fins increases the drag coefficient and drag force compared to adding one fin or without a fin.

## CHAPTER SIX

### 6.1 CONCLUSION AND RECOMMENDATION

#### 6.1.1 Conclusion

The Savonius wind turbine is powered by drag force. By adding a fin to the blade, the area of the turbine blades (turbine rotor) that capture the wind is divided, allowing the wind to be directed and fill the space in the blade more quickly. As a result, the turbine blades rotate at a slower rate than they would without the fin. The drag force that occurs along the blade area is likewise increased by the area of the split blade. The pressure along the blade area increases as the drag force acting on the blade increases, maximizing the pressure differential between the two turbine blades. At constant wind speed, the more fins added, the greater the pressure difference between the two blades. The positive drag force exerted on the blade increases as the pressure difference between the two blades increases. At a wind speed of  $2.15 \text{ m/s}$ , the drag force of two fins is greater than that of one fin and no fin. It means that adding two fins increases the power coefficient more effectively since the greater drag force results in a higher power coefficient value.

The drag and lift coefficients, as well as their corresponding forces, the aspect ratio, and the coefficient of power, are used to calculate the turbine's performance in this study. The turbine's performance in terms of coefficient of power is found to have a maximum value of  $C_p$  of 0.256, equivalent to a tip speed ratio of 0.7 at a twist angle of  $0^\circ$  at  $2.15 \text{ m/s}$  of wind speed, based on simulation outcomes.

Table 6. 1 Comparison of present studies with the previous studies

Different Literatures	Max. pressure (Kpa)				$C_p$
	Inlet velocity	No fin	One fin	Two fins	
Ridwan et al, 2019	5 m/s	101.343	101.340	101.344	0.241
Kumar & Saini, 2017	2 m/s	4.380	-	-	0.230
Present study	2.15 m/s	106.4	108.5	112.2	0.256



This paper founds that savonius wind turbine's performance is improved by altering the aspect ratios to minimal values and adding fins with the maximum number of two. Beyond this number the turbine will not rotate because of more friction between the blades and the rotor which indirectly affects the values of drag force. Finally, the research outcomes are drawn based on simulations for Savonius wind turbines without fin, with one and two fins:

- The addition of fins on the blade influences the value of the pressure and velocity distributions, as well as the drag coefficient. Among the data reviewed, blades with the addition of two fins produced a better pressure distribution than the others.
- For all tested scenarios, the pressure on concave blades is higher than on convex blades, and the blade with two fins is higher.
- The addition of a fin enhanced the drag coefficient. When compared to a blade without a fin and one fin, a blade with two fins show a higher drag coefficient/drag force.
- The power coefficient is influenced by the ratio between blade height and rotor diameter. A turbine with a lower aspect ratio has a higher power coefficient, according to the research.

### 6.1.2 Recommendation

More work should be done to acquire as many experimental samples as possible under diverse operating situations. Because this work lacks experimental analysis, it is recommended that experimental analysis be added. The goal should be to improve S-VAWT performance across a range of system parameters, including blade arc angle, blade shape factor, stage number, and operating factors including flow velocity, chord ratio, and overlap ratio. Detail study of the economic analysis of Savonius wind turbines need to be conducted compared with the other rural trends. A field study of size for S-VAWT should be carried out in the research locations to validate the outcomes of experimental and simulation studies.

## REFERENCE

- Akwa, J.V., Vielmo, H.A. and Petry, A.P. (2012) 'A review on the performance of Savonius wind turbines', *Renewable and Sustainable Energy Reviews*, 16(5), pp. 3054–3064. doi:10.1016/j.rser.2012.02.056.
- Anônimo (1994) 'Elements of Metric Gear Technology', pp. 1–124. Available at: <http://scholar.google.com/scholar?hl=en&btnG=Search&q=intitle:ELEMENTS+OF+METRIC+GEAR+TECHNOLOGY#0>.
- Argaw, N., Foster, R. and Ellis, A. (2003) 'Renewable Energy for Water Pumping Applications In Rural Villages; Period of Performance: April 1, 2001--September 1, 2001', *New Mexico State, United States* [Preprint], (July). Available at: <http://gisceu.net/PDF/U878.pdf%0Ahttp://www.osti.gov/servlets/purl/15004054-ydJAtT/native/>.
- B.U.Pai Wiley (2013) *Turbomachines*, ISBN: 978-81-265- -08046.
- B, D.G. *et al.* (2018) 'Pumping of Water by using Wind Turbine', pp. 416–418.
- Bisen, S. and Wasnik, A. (2019) 'Review paper on water pumping system using windmill', pp. 1962–1965.
- Brusca, S., Lanzafame, R. and Messina, M. (2014) 'Design of a vertical-axis wind turbine: how the aspect ratio affects the turbine's performance', *International Journal of Energy and Environmental Engineering*, 5(4), pp. 333–340. doi:10.1007/s40095-014-0129-x.
- Burton, T. *et al.* (2011) *Conceptual Design of Horizontal Axis Wind Turbines*, *Wind Energy Handbook*. doi:10.1002/9781119992714.ch6.
- Canonsburg, P. (2018) 'ANSYS CFX-Solver Theory Guide', (January). Available at: <http://www.ansys.com>.
- Contents, S. (no date) 'Section Contents Spur Gears', pp. 135–155.
- 'Dodota Spate Irrigation System Ethiopia A case study of' (2008), (November).
- Dumitrescu, O. *et al.* (2015) 'The renewable energy generated by the Savonius wind turbine used for water extraction', (January), pp. 141–146.
- Eesof, Agilent, V.B.B. (no date) *Machine Design Data Book*.
- Girma, M., Molina, M. and Assefa, A. (2015) 'Feasibility study of a wind powered water pumping system for rural Ethiopia', *AIMS Energy*, 3(4), pp. 851–868. doi:10.3934/energy.2015.4.851.

- Hadi Ali, M. (2013) 'Experimental Comparison Study for Savonius Wind Turbine of Two & Three Blades At Low Wind Speed', *International Journal of Modern Engineering Research (IJMER)* [www.ijmer.com](http://www.ijmer.com), 3(5), pp. 2978–2986.
- Hailu, A.D. and Kumsa, D.K. (2020) 'Ethiopia renewable energy potentials and current state', *AIMS Energy*, 9(1), pp. 1–14. doi:10.3934/ENERGY.2021001.
- Khurmi, R.S. and Gupta, J.K. (2005) 'A Textbook of Machine Design', *Garden*, (I), p. 14.
- Kumar, A. and Saini, R.P. (2017) *Performance analysis of a Savonius hydrokinetic turbine having twisted blades*, *Renewable Energy*. Elsevier Ltd. doi:10.1016/j.renene.2017.03.006.
- Kurniawan, Y., Dwi Prija Tjahjana, D.D. and Santoso, B. (2020) 'Experimental study of savonius wind turbine performance with blade layer addition', *Journal of Advanced Research in Fluid Mechanics and Thermal Sciences*, 69(1), pp. 23–33. doi:10.37934/ARFMTS.69.1.2333.
- Lukiyanto, Y.B. (2016) 'A Couple of Savonius Wind Mill and Centrifugal Reaction Pump as a Wind Energy Water Pump System', *Applied Mechanics and Materials*, 836, pp. 299–303. doi:10.4028/www.scientific.net/amm.836.299.
- Mahmoud, N.H. *et al.* (2012a) 'An experimental study on improvement of Savonius rotor performance', *Alexandria Engineering Journal*, 51(1). doi:10.1016/j.aej.2012.07.003.
- Mahmoud, N.H. *et al.* (2012b) 'An experimental study on improvement of Savonius rotor performance', *Alexandria Engineering Journal*, 51(1), pp. 19–25. doi:10.1016/j.aej.2012.07.003.
- Mariam, M.H. and Selassie, H. (2007) 'Ethiopia Country Report', (December), p. 25.
- Mondal, M.H.A. *et al.* (2018) 'Ethiopian universal electrification development strategies', *Intl Food Policy Res Inst.*, p. 4 pages. Available at: <http://ebrary.ifpri.org/cdm/ref/collection/p15738coll2/id/132767%0Ahttps://www.ifpri.org/publication/ethiopian-universal-electrification-development-strategies>.
- National, G. and Pillars, H. (no date) *Machine Design*.
- Pamungkas, S.F. *et al.* (2018) 'Performance "S" Type Savonius Wind Turbine with Variation of Fin Addition on Blade', *IOP Conference Series: Materials Science and Engineering*, 288(1). doi:10.1088/1757-899X/288/1/012132.
- Poluha, B.E. *et al.* (1990) 'CONCERN AN D An Evaluation of the Dodota Water Supply Project'.
- Pujari, P.C. *et al.* (2021) 'Performance enhancement of savonius turbine with the application of

reorienting blade mechanism', *Energy Sources, Part A: Recovery, Utilization and Environmental Effects*, 00(00), pp. 1–18. doi:10.1080/15567036.2021.1948635.

Ridwan, R., Setyawan, I. and Setiyono, S. (2019) 'Performance of vertical axis Savonius wind turbines related to the fin number on the blade', *IOP Conference Series: Materials Science and Engineering*, 539(1), pp. 2–9. doi:10.1088/1757-899X/539/1/012032.

Samiran, N.A. *et al.* (2014) 'Simulation study on the performance of vertical axis wind turbine', *Applied Mechanics and Materials*, 465–466(July 2015), pp. 270–274.

doi:10.4028/www.scientific.net/AMM.465-466.270.

Sanusi, A. *et al.* (2016) 'Experimental study of combined blade savonius wind turbine', *International Journal of Renewable Energy Research*, 6(2), pp. 615–619.

Saputro, H. *et al.* (2021) 'Numerical study of savonius wind turbines performance at Demak coastal area, Indonesia: A comparative study of savonius wind turbines without fin and with fin', *IOP Conference Series: Earth and Environmental Science*, 1808(1). doi:10.1088/1742-6596/1808/1/012026.

Talur, S., Kumar, K.P. and Madhusudhan, T. (2015) 'Review Paper of Savonius Vertical Axis Wind Turbine Rotor Blade', *Www.Ijmer.Com*, 5, pp. 7–14.

Tian, W. *et al.* (2015) 'Computational fluid dynamics prediction of a modified savonius wind turbine with novel blade shapes', *Energies*, 8(8), pp. 7915–7929. doi:10.3390/en8087915.

Utomo, I.S., Tjahjana, D.D.D.P. and Hadi, S. (2018) 'Experimental studies of Savonius wind turbines with variations sizes and fin numbers towards performance', *AIP Conference Proceedings*, 1931(February). doi:10.1063/1.5024100.

Wenehenubun, F., Saputra, A. and Sutanto, H. (2015) 'An experimental study on the performance of Savonius wind turbines related with the number of blades', *Energy Procedia*, 68, pp. 297–304. doi:10.1016/j.egypro.2015.03.259.

Zhou, T. and Rempfer, D. (2013) 'Numerical study of detailed flow field and performance of Savonius wind turbines', *Renewable Energy*, 51, pp. 373–381.

doi:10.1016/j.renene.2012.09.046.

## APPENDIX

### *Rotor stress calculation*

A windmill operates through forces that the wind exerts on its rotor. Those forces are then transferred to the load and the interaction between rotor and load causes various moments and forces in every part of the windmill structure.

### *Torque on a Rotor blade*

The torque available in the wind,  $T_w$  (Pujari *et al.*, 2021)

$$T_w = \frac{1}{2} * \rho * A_s * R * V^2 \Rightarrow R = \frac{D}{2} \quad (1)$$

$$T_w = \frac{1}{4} * \rho * A_s * D * V^2 \quad (2)$$

Where,

$\rho$  Density of air,  $1.1936 \frac{\text{Kg}}{\text{m}^3}$

$A_s$  Swept area,  $6.4 \text{ m}^2$

$D$  Rotor diameter,  $3 \text{ m}$

$V$  Wind speed,  $2.15 \frac{\text{m}}{\text{s}}$

Substituting the values into Equation 2,  $T_w = 26.48 \text{ Nm}$

The torque on the rotor,  $T_r$  is calculated (Hadi Ali, 2013)

$$T_r = T_w * C_t \quad (3)$$

Where,

$$C_t \quad \text{torque coefficient, } \frac{C_p}{\lambda} = \frac{0.32}{0.7} = 0.457 \quad (4)$$

$$T_r = 12.10 \text{ Nm}$$

### *Power Transmission Mechanism*

Gears, shafts, and bearings are the essential transmission mechanisms used in engineering processes. They are the most important elements used in gearboxes, drive trains, and transmissions.

#### *Gear*

Gear is a wheel-like component with evenly spaced teeth around its outer periphery that engages another toothed mechanism to modify the speed or direction of transmitted motion. Gears are mounted on rotational shafts, and the teeth of one gear mesh with the teeth of the other, causing the rotary motion to be transmitted. Torque is also transferred from one portion of the machine to the other because of this.

The following requirements must be considered while using gears:

- ✓ To transmit motion from one shaft to another
- ✓ Be widely available
- ✓ Be easy to fabricate and hence economically viable
- ✓ High transmission efficiency

#### *Design of Gears*

Gears are mounted on rotatable shafts with the teeth on one gear meshing with the teeth of the other gear. A spur gear is selected based on the following factors (Eesof, Agilent, no date).

- ✓ The general layout of shafts
- ✓ Speed reduction
- ✓ Power to be transmitted
- ✓ Input speed
- ✓ Cost

The selected material is mild steel which is a ferrous metal made from iron and carbon (ferromagnetic).

It has the following properties

- ✓ Excellent weldability and machinable or ductile
- ✓ Not responsive to heat treatment
- ✓ Comparatively low cost
- ✓ Has good magnetic properties due to its high iron content

Mechanical properties

Allowable stress,  $\sigma_{all} = 275$  MPa

Allowable bending stress,  $\sigma_b = 248$  MPa

Ultimate tensile strength,  $\sigma_{ut} = 400 \frac{N}{mm^2}$

Shear stress,  $\tau = 250$  MPa

Young's modulus = 200 GPA

BHN = 200

Table 1 Efficiencies of various types of Gears and their standard Gear Ratios (Contents, no date)

Types of Gear	Standard gear ratio	Efficiency of gear
Spur	1:1 to 6:1	95-99%
Helical	1:1 to 10:1	97-99%
Bevel	1:1 to 4:1	96-99%

From standards

All standard systems prescribe the involute profile than the cycloidal profile for gear tooth. The reasons are

- ✓ The involute profile satisfies the fundamental law of gearing at any center distance.
- ✓ All involute gears of a given module and pressure angle are interchangeable.
- ✓ All involute gears of a given module and pressure angle can be machined from one single tool (Eesof, Agilent, no date)

There are three standard systems for the shape of gear teeth. They are

- 14.5° full depth involute system
- 20° full depth involute system
- 20° stub involute system



Among those standards, the 20° full depth involute pressure angle system is selected because of the following advantages over other types of pressure angle systems:

- ✓ It reduces the risk of undercutting and interference.
- ✓ Due to the increased pressure angle, the tooth becomes slightly broader at the root. This makes the tooth stronger and increases the load-carrying capacity.
- ✓ It has a greater length of contact (Eesof, Agilent, no date)

To calculate the diameter of gear and pinion, a module is a major factor, which determines the size of gear (Eesof, Agilent, no date) The module,  $m$  specifies the size of the gear tooth, which means as the module increases, the size of the gear tooth also increases. A larger tooth size enables more power to be transmitted and mating gears must have the same module. It is calculated from the diametral pitch. The diametral pitch ( $P_d$ ) is the ratio of the number of teeth on gear to the diameter of gear or the ratio of the number of teeth of the pinion to the diameter of the pinion. The module is expressed in mm.

$$m = \frac{25.4}{P_d} \text{ where, } P_d = \frac{T_g}{D_g} = \frac{T_p}{D_p} \quad (5)$$

The actual sizes of 20°-pressure-angle, standard, full-depth teeth from  $P_d = 4$  to 80.

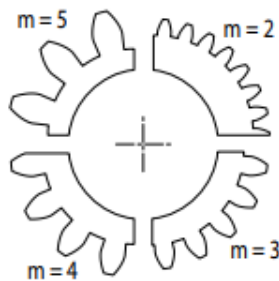


Figure 1 Module (Eesof, Agilent, no date)

Assumptions of the tooth forms are standard AGMA full-depth involute profiles (Eesof, Agilent, no date)

Based on the above standards, taking  $P_d = 6$ , pressure angle  $\phi = 20^\circ$ , and from gear efficiency table gear ratio,  $GR = 3:1$

Using those data, the number of teeth on the gear,  $T_g$

The number of teeth on the pinion ( $T_p$ ) to avoid interference is obtained from

$$T_p = \frac{2*Aw}{GR[\sqrt{1+\frac{1}{GR}(\frac{1}{GR}+2)\sin^2 \phi}-1]} \quad (6)$$

Aw = fraction by which the standard addendum for the gear multiplied

GR= gear ratio, 3 and  $\phi$  = pressure angle,  $20^\circ$

$$T_p = \frac{2*1}{3*[\sqrt{1+\frac{1}{3}(\frac{1}{3}+2)\sin^2 20}-1]} = 15 \dots \text{Minimum number of pinion teeth (Khurmi and Gupta, 2005)}$$

Then take a number of teeth on the pinion,  $T_p = 19$

$$GR = \frac{T_g}{T_p} \Rightarrow T_g = GR * T_p \Rightarrow 3 * 19 = 57 \text{ teeth} \quad (7)$$

$$\text{Module, } m = \frac{25.4}{P_d} \Rightarrow \frac{25.4}{6} = 4 \text{ mm} \quad (8)$$

To determine the diameter of the gear and pinion follow the following steps.

$$\text{Diameter of gear, } D_g = \text{module} * \text{teeth of gear} = m * T_g = 4 \text{ mm} * 57 = 0.228 \text{ m} \quad (9)$$

$$\text{Diameter of pinion, } D_p = \text{module} * \text{teeth of pinion} = m * T_p = 4 \text{ mm} * 19 = 0.076 \text{ m} \quad (10)$$

Angular velocity of the pinion gear,

$$\omega_p = \frac{\lambda * V}{R} = \frac{0.7 * 2.15 \frac{\text{m}}{\text{s}}}{1.5 \text{ m}} = 1.003 \frac{\text{rad}}{\text{s}} \quad (11)$$

In another way, angular velocity is written as

$$\omega = \frac{2\pi N}{60} \quad (12)$$

From equation 12, the speed of pinion gear,  $N_p$  and the Speed of gear,  $N_g$  values are 10 rpm and 3.3 rpm respectively.

Also from equation 12, the angular velocity of gear,  $\omega_g = 0.35 \frac{\text{rad}}{\text{s}}$

Standard proportions of the gear tooth for  $20^\circ$  full depth system in terms of module....Table D

Addendum,  $a = m = 4 \text{ mm}$

Dedendum,  $d = 1.25 m = 1.25 * 4 \text{ mm} = 5 \text{ mm}$

Clearance,  $c = 0.25 * m = 0.25 * 4 \text{ mm} = 1 \text{ mm}$  or  $d - a = 5 \text{ mm} - 4 \text{ mm} = 1 \text{ mm}$

Working depth,  $h_k = 2 * m = 2 * 4 \text{ mm} = 8 \text{ mm}$

Whole depth,  $h_t = 2.25 * m = 2.25 * 4 \text{ mm} = 9 \text{ mm}$

Tooth thickness =  $1.571 * m = 1.571 * 4 \text{ mm} = 6.284 \text{ mm}$

Tooth space =  $1.571 * m = 1.571 * 4 \text{ mm} = 6.284 \text{ mm}$

Fillet radius  $0.4 * m = 0.4 * 4 \text{ mm} = 1.6 \text{ mm}$

Center distance,  $C = \frac{m(T_p + T_g)}{2}$  or  $\frac{D_p + D_g}{2} = \frac{4 \text{ mm}(19+57)}{2}$  or  $\frac{228 \text{ mm} + 76 \text{ mm}}{2} = 152 \text{ mm}$

Power input to the shaft of gearbox,  $P_{sg} = 11.21 \text{ W}$

Torque on the pinion shaft

$$T_p = \frac{P_{sg}}{\omega_p} = \frac{P_{sg} * 60}{2\pi N_p} = \frac{11.21 \text{ W} * 60}{2\pi * 10 \text{ rpm}} = 11 \text{ N-m}$$

Torque on the gear,  $T_g$  from gear ratio GR

$$GR = \frac{T_g}{T_p}$$

$$T_g = GR * T_p = 3 * 11 \text{ N-m} = 33 \text{ N-m}$$

The load  $W$  exerted on gear and pinion is equal and opposite.

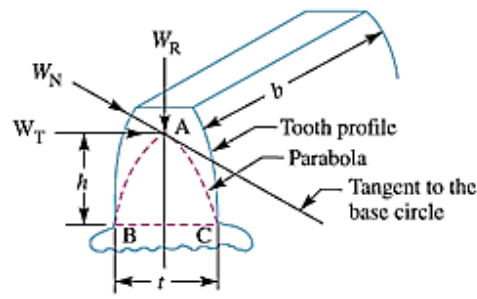


Figure 2 Tooth of Gear (Khurmi and Gupta, 2005)

Tangential tooth force,  $W_T$

$$W_T = \frac{T_g}{r_g} = \frac{T_p}{r_p} \text{ OR } \frac{2 * T_g}{D_g} = \frac{2 * T_p}{D_p} \quad (13)$$

Where  $T_g$  and  $T_p$  are torque on gear and pinion respectively

$D_g$ , diameter of gear = 228 mm = 0.228 m and

$D_p$ , diameter of pinion = 76 mm = 0.076 m

From equation 12,  $W_T = 289.5 \text{ N}$  (Same and opposite for both gear and pinion)

Radial tooth force,  $W_R$  is

$$W_R = W_T \tan \phi = 289.5 \text{ N} * \tan 20 \quad (14)$$

$W_R = 105.4 \text{ N}$  (Same and opposite for both Gear and Pinion)

Normal load,  $W_N$

$$W_N = \frac{W_T}{\cos \phi} \text{ or } \sqrt{(W_T)^2 + (W_R)^2} \Rightarrow \frac{289.5 \text{ N}}{\cos 20} \text{ or } \sqrt{(289.5 \text{ N})^2 + (105.4 \text{ N})^2} \quad (15)$$

$$W_N = 308.1 \text{ N}$$

*Effective Load on Gear Tooth,  $P_{eff}$*

$$P_{eff} = \text{Static load} + \text{Dynamic load} = P_s + P_d \quad (16)$$

Where,  $P_s = W_T * C_s$

$W_T$ , Tangential tooth force = 289.5 N

$C_s$  = service factor = 1.5 for uniform load.....Table F

Static load,  $P_s = 289.5 \text{ N} * 1.5 = 434.25 \text{ N}$

$$\text{Dynamic load, } P_d = \frac{21v (Ceb+W_T)}{21v + \sqrt{(Ceb+W_T)}} \quad (17)$$

Where,  $b$  = face width = 40 mm

$C$  = deformation factor,  $\frac{N}{mm^2}$

$$C = \frac{K}{\frac{1}{E_g + E_p}}, \text{ K = constant value depending upon the form of tooth} = 0.111$$

Table 2 Values of K for various tooth forms (Eesof, Agilent, no date)

K = 0.107	For 14.5° full depth teeth
K = 0.111	For 20° full depth teeth
K = 0.115	For 20° stub teeth

$$C = \frac{0.111}{\frac{1}{200,000 \frac{N}{mm^2} + 200,000 \frac{N}{mm^2}}} = 11,100 \frac{N}{mm^2}$$

$e$  = sum of errors between two meshing teeth (depends on the quality of the gears and technique of manufacturing. There are 12 different grades, in decreasing order of precision.).....Table I

$$e = e_p + e_g$$

Taking Grade 10 for machining accuracy

$$\text{Tolerance in adjacent pitch for grade 10 accuracy} = 32 + 2.5 \phi \quad (18)$$

$$\text{Tolerance factor, } \phi = m + 0.25\sqrt{d}$$

Module,  $m = 4$  mm and  $d =$  diameter, mm

Pinion

$$d_p = 76 \text{ mm}$$

$$\phi_p = m + 0.25\sqrt{d_p} = 4 \text{ mm} + 0.25\sqrt{76} \text{ mm} = 6.18$$

$$e_p = 32 + 2.5\phi_p = 32 + 2.5*6.18$$

$$e_p = 47.45 \text{ microns}$$

Gear

$$d_g = 228 \text{ mm}$$

$$\phi_g = m + 0.25\sqrt{d_g} = 4 \text{ mm} + 0.25\sqrt{228} \text{ mm} = 7.775$$

$$e_g = 32 + 2.5\phi_g = 32 + 2.5*7.775$$

$$e_g = 51.44 \text{ microns}$$

$$e = e_p + e_g = 47.45 \text{ microns} + 51.44 \text{ microns}$$

$$e = 98.89 \text{ microns} = 0.09889 \text{ mm}$$

$$\text{Pitch line velocity, } v = \frac{d_p \omega_p}{2} = \frac{0.076 \text{ m} * 1.003 \frac{\text{rad}}{\text{s}}}{2} = 0.038 \frac{\text{m}}{\text{s}}$$

Then, the dynamic load becomes

$$P_d = \frac{21v (Ceb+W_T)}{21v + \sqrt{(Ceb+W_T)}} = \frac{21*0.038 \frac{\text{m}}{\text{s}} (11,100 \frac{\text{N}}{\text{mm}^2} * 0.09889 \text{ mm} * 40 \text{ mm} + 289.5 \text{ N})}{21*0.038 \frac{\text{m}}{\text{s}} + \sqrt{(11,100 \frac{\text{N}}{\text{mm}^2} * 0.09889 \text{ mm} * 40 \text{ mm} + 289.5 \text{ N})}} = 167.1 \text{ N}$$

Finally,

$$P_{\text{eff}} = P_s + P_d = 434.25 \text{ N} + 167.1 \text{ N}$$

$$P_{\text{eff}} = 601.35 \text{ N}$$

*Beam strength of gear tooth,  $S_b$*

The maximum value of the tangential force that the tooth can transmit without bending failure. It is calculated using Lewis's equation.

Lewis took the following assumptions (National and Pillars, no date)

- ✓ Tangential load is uniformly distributed along the face width of the tooth.
- ✓ The effect of stress concentration at the root of the tooth is neglected.
- ✓ Radial load is much smaller in comparison to tangential load and its effect is neglected.
- ✓ At any time of power transmission, only one pair of teeth is in contact.
- ✓ The effect of the radial component, which induces compressive stresses, is neglected.

Beam strength of gear tooth,  $S_b = mbY\sigma_b$  (19)

Where, Module,  $m = 4$  mm

Face width,  $b = 10m = 10 * 4$  mm = 40 mm

$Y =$  Lewis form factor .....from table 4 (The design is based on the weaker of the two gears, that is, pinion having lesser number of teeth and lesser value of  $Y$ .)

$Y = 0.314$  for 19 number of teeth

$\sigma_b =$  allowable bending stress ( $\frac{N}{mm^2}$ )

$$\sigma_b = \frac{1}{3} \sigma_{ut} \left( \sigma_{ut} = 400 \frac{N}{mm^2} \right)$$

$$\sigma_b = \frac{1}{3} * 400 \frac{N}{mm^2} = 133.33 \frac{N}{mm^2}$$

Using equation 19, the beam strength,  $S_b = 6698.5$  N

For safe design,  $S_b \geq P_{eff}$

Therefore, the design is safe.

Wear strength of gear tooth,  $S_w$

The maximum value of the tangential force that the tooth can transmit without pitting failure. It is calculated using Buckingham's equation.

$$S_w = bQKD_p \quad (20)$$

Where  $S_w$  = tangential strength due to wear

$$Q = \text{ratio factor } (Q = \frac{2T_g}{T_g + T_p} = \frac{2D_g}{D_g + D_p}) = \frac{2 \cdot 57}{19 + 57} = 1.5$$

$$K = \text{stress-load factor, } \frac{N}{mm^2} = \frac{(\sigma_c)^2 \sin \phi \cos \phi (\frac{1}{E_p} + \frac{1}{E_g})}{1.4}$$

$E_p$  and  $E_g$  = modulus of elasticity for pinion and gear materials respectively

$$E_p = E_g = 200,000 \frac{N}{mm^2} \text{ since they have the same material}$$

$\phi$  = pressure angle =  $20^\circ$

$b$  = Face width = 40 mm

$D_p$  = Diameter of pinion = 76 mm

$\sigma_c$  = surface endurance strength of the material ( $\frac{N}{mm^2}$ )

$$\sigma_c = 0.27(9.81) \text{ (BHN)} \frac{N}{mm^2} \dots \text{according to G. Niemen (Kurniawan, Dwi Prija$$

Tjahjana and Santoso, 2020)

BHN = Brinell Hardness Number (surface hardness of gears) = 200

$$\sigma_c = 0.27(9.81) \text{ (BHN)} = 0.27 \cdot 9.81 \cdot 200 = 530 \frac{N}{mm^2}$$

$$\text{Then stress-load factor, } K = \frac{(530 \frac{N}{mm^2})^2 \sin 20 \cos 20 (\frac{1}{200,000 \frac{N}{mm^2}} + \frac{1}{200,000 \frac{N}{mm^2}})}{1.4} = 0.645 \frac{N}{mm^2}$$

Using equation 20, the tangential wear strength,  $S_w = 2941.2 \text{ N}$

For safe design,  $S_w \geq P_{\text{eff}}$

Therefore, the design is safe.

### *Shaft*

A shaft is a rotating member, usually of circular cross-section, used to transmit power or motion. It provides the axis of rotation of the elements such as gears, pulleys, etc., and control of the geometry of motion. Shafts are manufactured by hot rolling, cold drawing, or turning and grinding.

### Types of Shafts

- Transmission shafts- These shafts transmit power between the source and the machines absorbing power. The countershafts, line shafts, overhead shafts, and all factory shafts are transmission shafts. Since these shafts carry machine parts such as pulleys, gears, etc., therefore they are subjected to bending in addition to twisting.
- Machine shafts- These shafts form an integral part of the machine itself.

E.g. Crankshaft

### *Design of shaft*

Experimental investigations suggest that the Maximum Shear Stress Theory gives good predictions for ductile materials. Shafts are made of ductile material like steel and therefore, this theory applies to shaft design (Eesof, Agilent, no date)

Maximum Shear Stress Theory,  $\tau_{max}$

$$\tau_{max} = \frac{16}{\pi d^3} \sqrt{M^2 + T^2} \quad (21)$$

Where, M = bending moment and T = torque on the gear and pinion

$$\tau_{max} = \frac{0.5 \sigma_{yt}}{FS}$$

One important approach to designing a transmission shaft is to use the ASME code. According to this code, the permissible shear stress  $\tau_{max}$  for the shaft without keyways is taken as

$$\tau_{max} = 0.30 \sigma_{yt} \text{ or } \tau_{max} = 0.18 \sigma_{ut} \text{ (whichever is minimum)}$$

$\sigma_{yt}$  = Yield strength and  $\sigma_{ut}$  = Ultimate tensile strength of the material

If keyways are present, the above value is reduced by 25 percent.

$$\tau_{max} = 0.225 \sigma_{yt} = 0.135 \sigma_{ut} \text{ when keyways are present}$$



ASME code

$$\tau_{max} = \frac{16}{\pi d^3} \sqrt{(K_b M)^2 + (K_t T)^2} \quad (22)$$

Where  $K_b$  = combined shock and fatigue factor applied to bending moment

$K_t$  = combined shock and fatigue factor applied to torque

Table 3 Values of shock and fatigue factors  $K_b$  and  $K_t$  (Eesof, Agilent, no date)

Application	$K_b$	$K_t$
Load gradually applied	1.5	1.0
Load suddenly applied (minor shock)	1.5-2.0	1.0-1.5
Load suddenly applied (heavy shock)	2.0-3.0	1.5-3.0

### Selection of material

Solid steel shaft with properties of  $\sigma_{yt} = 250 \frac{N}{mm^2}$  and  $\sigma_{ut} = 550 \frac{N}{mm^2}$

### Diameter of Gear or input shaft

Normal load acting between the tooth surfaces,  $W_N = 308.1 \text{ N}$ .

The weight of the Gear,  $W_G$  (Khurmi and Gupta, 2005)

$$W_G = 0.00118 T_g b m^2 \quad (23)$$

Where,  $T_g$  = number of gear teeth = 57

$b$  = face width = 40 mm

$m$  = module = 4 mm

Using equation 23,  $W_G = 43.05 \text{ N}$

The resultant load acting on the gear,  $W_R$

$$W_R = \sqrt{(W_N)^2 + (W_G)^2 + 2W_N W_G \cos \phi} = \sqrt{(308.1 \text{ N})^2 + (43.05 \text{ N})^2 + 2 * 43.05 \text{ N} * 308.1 \text{ N} \cos 20}$$

$$W_R = 348.86 \text{ N}$$

The bending moment on the shaft due to the resultant load,  $M$

$M = W_R * L$  where,  $L$  = the distance between the center of the Gear and Bearing = 50 mm

$$M = 348.86 \text{ N} * 50 \text{ mm} = 17,443 \text{ N-mm}$$

The shaft is under the combined effect of torsion and bending, therefore equivalent torque is calculated, as

$$T_e = \sqrt{(K_b M)^2 + (K_t T)^2} \text{ Where } T = \text{torque on the gear} = 33,000 \text{ N-mm} \quad (24)$$

$$K_b = 1.5 \text{ and } K_t = 2$$

Using equation 24,  $T_e = 70,997.05 \text{ N-mm}$

The diameter of the gear shaft (d) using the ASME code

$$T_e = \frac{\pi}{16} * \tau_{max} * d^3$$

Gears are fitted on the shaft with the help of keys.

$$\tau_{max} = 0.225 \sigma_{yt} = 0.225 * 250 \frac{\text{N}}{\text{mm}^2} = 56.25 \frac{\text{N}}{\text{mm}^2}$$

$$\tau_{max} = 0.135 \sigma_{ut} = 0.135 * 550 \frac{\text{N}}{\text{mm}^2} = 74.25 \frac{\text{N}}{\text{mm}^2}$$

Taking the minimum value,  $\tau_{max} = 56.25 \frac{\text{N}}{\text{mm}^2}$

Diameter of the input shaft

$$d^3 = \frac{T_e * 16}{\pi * \tau_{max}} = \frac{70,997.05 \text{ N-mm} * 16}{\pi * 56.25 \frac{\text{N}}{\text{mm}^2}} = 20 \text{ mm}$$

*Diameter of pinion or output shaft*

Normal load acting between the tooth surfaces,  $W_N = 308.1 \text{ N}$

$$W_P = 0.00118 T_p b m^2 = 0.00118 * 19 * 40 \text{ mm} * (4 \text{ mm})^2 = 14.35 \text{ N}$$

The resultant load acting on the pinion,  $W_R$

$$W_R = \sqrt{(W_N)^2 + (W_P)^2 + 2 W_N W_P \cos \phi} = \sqrt{(308.1 \text{ N})^2 + (14.35 \text{ N})^2 + 2 * 14.35 \text{ N} * 308.1 \text{ N} \cos 20}$$

$$W_R = 321.6 \text{ N}$$

The bending moment, M

$$M = W_R * L$$

Where, L = the distance between the center of the pinion and Bearing = 50 mm

$$M = 321.6 \text{ N} * 50 \text{ mm} = 16,080 \text{ N-mm}$$

Equivalent torque,  $T_e$

$$T_e = \sqrt{(K_b M)^2 + (K_t T)^2} \text{ Where } T = \text{torque on the pinion} = 11,000 \text{ N-mm} \quad (25)$$

$$K_b = 1.5 \text{ and } K_t = 2$$

Using equation 25,  $T_e = 32,646.2 \text{ N-mm}$

Finally, the diameter of the output shaft (d) using the ASME code

$$T_e = \frac{\pi}{16} * \tau_{max} * d^3$$
$$d^3 = \frac{T_e * 16}{\pi * \tau_{max}} = \frac{32,646.2 \text{ N-mm} * 16}{\pi * 56.25 \frac{\text{N}}{\text{mm}^2}} = 14 \text{ mm}$$

### Key

A key is an axially fitted machine part, such as pulleys or gears that fit into the mating member. To prevent relative rotation between the shaft and the mating part, it is always inserted parallel to the axis of the shaft. They are used as temporary fasteners and are subjected to many crushing and shearing forces. A keyway is a slot or depression in the shaft and hub of a pulley or gear that allows a key to fit.

Keys that are commonly used

- Square key: A square key is sunk half in the shaft and half in the hub of a gear, pulley, or crank. Its sides are one-fourth of the shaft diameter.
- Rectangular (flat) Key: Rectangular or flat keys are utilized where the shaft is severely weakened and additional connection stability is necessary, such as in machine tools.
  - ✓ Feather keys: Flat keys with a uniform cross-section that allow the hub to rotate axially on the shaft.
  - ✓ Tapered keys: They have a gib head that allows them to be removed when the other end is unavailable.
- Saddle key: Saddle keys only fit in the hub's keyway; there is no keyway on the shaft. They are suited for light service or where relative motion between the shaft and the hub is required for adjustment and the keyway on the shaft is not available.
- Woodruff key: A woodruff key is a sunk key with an approximately semi-circular disk of uniform thickness that may be adjusted. The wider key-way depth prevents the key from slipping over the shaft but also weakens the shaft much more than using straight keys.
- Tangent Key: Tangent keys are made up of two sections, each of which is tapered for a secure fit.

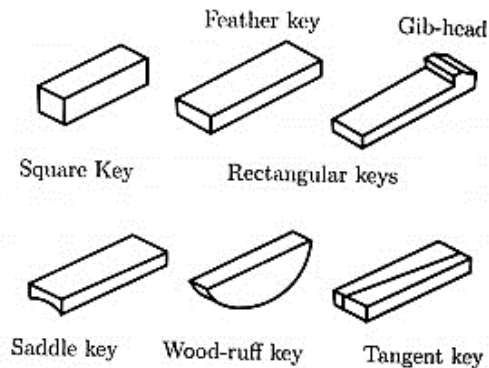


Figure 1: Types of Keys

Figure 3 Types of Keys (Khurmi and Gupta, 2005)

### *Selection of key*

The selection of the type of key for a given application depends upon the following factors:

- ✓ Power to be transmitted
- ✓ Tightness of fit
- ✓ Stability of connection; and
- ✓ Cost

For this design, a rectangular flat key is selected due to its stability, simplicity in design, and manufacturing.

### Key for the input shaft

Shaft diameter,  $d = 20$  mm

Torque on the gear,  $T = 33$  Nm

### Material selection

- ✓ Steel with a yield stress,  $\sigma_y = 250$  MPa and  $\sigma_{ut} = 550$  MPa
- ✓ Take factor of safety,  $F.S = 2$

For shaft diameter of 20 mm from the standard table of a selection of rectangular flat keys....

### Table G

Width,  $W = 8$  mm,

Thickness,  $t = 7$  mm, and

Length,  $l = 1.5 d = 1.5 * 20$  mm = 30 mm

Due to the power transmitted by the shaft, the key may fail due to shear stress and compressive stress.

$$\text{Maximum shear stress, } \tau_{max} = \frac{0.5 \sigma_y}{F.S} = \frac{0.5 * 250 \text{ MPa}}{2} = 62.5 \text{ MPa}$$

The torque transmitted by the shaft using a diameter of 20 mm is  $T = 33,000 \text{ N-mm}$ .

Considering the failure of the key due to shear stress,

$$\tau = \frac{2T}{d * w * l} = \frac{2 * 33,000 \text{ Nmm}}{20 \text{ mm} * 8 \text{ mm} * 30 \text{ mm}} = 13.75 \text{ MPa}$$

$\tau < \tau_{max}$ , this implies that the design is safe against shearing stress.

Maximum compressive stress,  $\sigma_c = 2\tau_{max} = 2 * 62.5 \text{ MPa} = 125 \text{ MPa}$

Considering the failure of keys due to compressive stress.

$$\sigma = \frac{4T}{d * t * l} = \frac{4 * 33,000 \text{ Nmm}}{20 \text{ mm} * 7 \text{ mm} * 30 \text{ mm}} = 31.43 \text{ MPa}$$

$\sigma < \sigma_c$ , this shows the key is safe against compressive stress (crushing).

Key for output shaft

Shaft diameter,  $d = 14 \text{ mm}$

for shaft diameter of 14 mm from the standard table of a selection of rectangular flat keys... Table G

Width,  $W = 6 \text{ mm}$

Thickness,  $t = 5 \text{ mm}$ , and

Length,  $l = 1.5 d = 1.5 * 14 \text{ mm} = 21 \text{ mm}$

Due to the power transmitted by the shaft, the key may fail due to shear stress and compressive stress.

$$\text{Maximum shear stress, } \tau_{max} = \frac{0.5 \sigma_y}{F.S} = \frac{0.5 * 250 \text{ MPa}}{2} = 62.5 \text{ MPa}$$

The torque transmitted by the shaft using a diameter of 14 mm is  $T = 11,000 \text{ N-mm}$ .

Considering the failure of the key due to shear stress,

$$\tau = \frac{2T}{d * w * l} = \frac{2 * 11,000 \text{ Nmm}}{14 \text{ mm} * 6 \text{ mm} * 21 \text{ mm}} = 12.47 \text{ MPa}$$

$\tau < \tau_{max}$ , the design is safe against shearing stress.

Maximum compressive stress,  $\sigma_c = 2\tau_{max} = 2 * 62.5 \text{ MPa} = 125 \text{ MPa}$

Considering the failure of keys due to compressive stress.

$$\sigma = \frac{4T}{d*t*l} = \frac{4*11,000 \text{ Nmm}}{14 \text{ mm}*5 \text{ mm}*21 \text{ mm}} = 29.93 \text{ MPa}$$

The key is safe against compressive stress or crushing ( $\sigma < \sigma_c$ )

### *Selection of Bearing*

Bearing is a mechanical element that permits relative motion between two parts, such as the shaft and the housing, with minimum friction. The functions of the bearing are as follows:

- ✓ The bearing ensures free rotation of the shaft or the axle with minimum friction.
- ✓ The bearing supports the shaft or the axle and holds it in the correct position.
- ✓ The bearing takes up the forces that act on the shaft or the axle and transmits them to the frame or the foundation.

Bearings are classified depending upon

1. The direction of the force that acts on them
  - ✓ Radial bearing and
  - ✓ Thrust bearings
2. Type of friction between the shaft and the bearing surface
  - ✓ Sliding contact bearings (plain bearings) and
  - ✓ Rolling contact bearings (ball bearings)

Roller/ball bearings are used to support the shaft at the ends.

### *Advantages*

- ✓ Low starting and running friction except at very high speeds
- ✓ Ability to withstand momentary shock loads
- ✓ Support combined loads (radial and axial loads)
- ✓ Accuracy of shaft alignment
- ✓ Low cost of maintenance, as no lubrication is required while in service
- ✓ Small overall dimensions
- ✓ Reliability of service
- ✓ Easy to mount and erect
- ✓ Cleanliness

Disadvantages

- ✓ Noisier at very high speeds
- ✓ Low resistance to shock loading
- ✓ More initial cost

From Table H deep groove ball bearing having code 61804 with outer diameter,  $D_o = 32$  mm and width,  $B = 7$  mm is selected for the input shaft diameter of 20 mm.

Similarly, for the output shaft of diameter 14 mm deep groove ball bearing having code 61802 with outer diameter,  $D_o = 24$  mm and width,  $B = 5$  mm is selected.

Table A Property table for Air at 1 atm pressure

**PROPERTY TABLES AND CHARTS**

**TABLE A-9**

Properties of air at 1 atm pressure

Temp. <i>T</i> , °C	Density $\rho$ , kg/m <sup>3</sup>	Specific Heat $c_p$ J/kg·K	Thermal Conductivity $k$ , W/m·K	Thermal Diffusivity $\alpha$ , m <sup>2</sup> /s	Dynamic Viscosity $\mu$ , kg/m·s	Kinematic Viscosity $\nu$ , m <sup>2</sup> /s	Prandtl Number Pr
-150	2.866	983	0.01171	$4.158 \times 10^{-6}$	$8.636 \times 10^{-6}$	$3.013 \times 10^{-6}$	0.7246
-100	2.038	966	0.01582	$8.036 \times 10^{-6}$	$1.189 \times 10^{-5}$	$5.837 \times 10^{-6}$	0.7263
-50	1.582	999	0.01979	$1.252 \times 10^{-5}$	$1.474 \times 10^{-5}$	$9.319 \times 10^{-6}$	0.7440
-40	1.514	1002	0.02057	$1.356 \times 10^{-5}$	$1.527 \times 10^{-5}$	$1.008 \times 10^{-5}$	0.7436
-30	1.451	1004	0.02134	$1.465 \times 10^{-5}$	$1.579 \times 10^{-5}$	$1.087 \times 10^{-5}$	0.7425
-20	1.394	1005	0.02211	$1.578 \times 10^{-5}$	$1.630 \times 10^{-5}$	$1.169 \times 10^{-5}$	0.7408
-10	1.341	1006	0.02288	$1.696 \times 10^{-5}$	$1.680 \times 10^{-5}$	$1.252 \times 10^{-5}$	0.7387
0	1.292	1006	0.02364	$1.818 \times 10^{-5}$	$1.729 \times 10^{-5}$	$1.338 \times 10^{-5}$	0.7362
5	1.269	1006	0.02401	$1.880 \times 10^{-5}$	$1.754 \times 10^{-5}$	$1.382 \times 10^{-5}$	0.7350
10	1.246	1006	0.02439	$1.944 \times 10^{-5}$	$1.778 \times 10^{-5}$	$1.426 \times 10^{-5}$	0.7336
15	1.225	1007	0.02476	$2.009 \times 10^{-5}$	$1.802 \times 10^{-5}$	$1.470 \times 10^{-5}$	0.7323
20	1.204	1007	0.02514	$2.074 \times 10^{-5}$	$1.825 \times 10^{-5}$	$1.516 \times 10^{-5}$	0.7309
25	1.184	1007	0.02551	$2.141 \times 10^{-5}$	$1.849 \times 10^{-5}$	$1.562 \times 10^{-5}$	0.7296
30	1.164	1007	0.02588	$2.208 \times 10^{-5}$	$1.872 \times 10^{-5}$	$1.608 \times 10^{-5}$	0.7282
35	1.145	1007	0.02625	$2.277 \times 10^{-5}$	$1.895 \times 10^{-5}$	$1.655 \times 10^{-5}$	0.7268
40	1.127	1007	0.02662	$2.346 \times 10^{-5}$	$1.918 \times 10^{-5}$	$1.702 \times 10^{-5}$	0.7255
45	1.109	1007	0.02699	$2.416 \times 10^{-5}$	$1.941 \times 10^{-5}$	$1.750 \times 10^{-5}$	0.7241
50	1.092	1007	0.02735	$2.487 \times 10^{-5}$	$1.963 \times 10^{-5}$	$1.798 \times 10^{-5}$	0.7228
60	1.059	1007	0.02808	$2.632 \times 10^{-5}$	$2.008 \times 10^{-5}$	$1.896 \times 10^{-5}$	0.7202
70	1.028	1007	0.02881	$2.780 \times 10^{-5}$	$2.052 \times 10^{-5}$	$1.995 \times 10^{-5}$	0.7177
80	0.9994	1008	0.02953	$2.931 \times 10^{-5}$	$2.096 \times 10^{-5}$	$2.097 \times 10^{-5}$	0.7154
90	0.9718	1008	0.03024	$3.086 \times 10^{-5}$	$2.139 \times 10^{-5}$	$2.201 \times 10^{-5}$	0.7132
100	0.9458	1009	0.03095	$3.243 \times 10^{-5}$	$2.181 \times 10^{-5}$	$2.306 \times 10^{-5}$	0.7111
120	0.8977	1011	0.03235	$3.565 \times 10^{-5}$	$2.264 \times 10^{-5}$	$2.522 \times 10^{-5}$	0.7073
140	0.8542	1013	0.03374	$3.898 \times 10^{-5}$	$2.345 \times 10^{-5}$	$2.745 \times 10^{-5}$	0.7041
160	0.8148	1016	0.03511	$4.241 \times 10^{-5}$	$2.420 \times 10^{-5}$	$2.975 \times 10^{-5}$	0.7014
180	0.7788	1019	0.03646	$4.593 \times 10^{-5}$	$2.504 \times 10^{-5}$	$3.212 \times 10^{-5}$	0.6992
200	0.7459	1023	0.03779	$4.954 \times 10^{-5}$	$2.577 \times 10^{-5}$	$3.455 \times 10^{-5}$	0.6974
250	0.6746	1033	0.04104	$5.890 \times 10^{-5}$	$2.760 \times 10^{-5}$	$4.091 \times 10^{-5}$	0.6946
300	0.6158	1044	0.04418	$6.871 \times 10^{-5}$	$2.934 \times 10^{-5}$	$4.765 \times 10^{-5}$	0.6935
350	0.5664	1056	0.04721	$7.892 \times 10^{-5}$	$3.101 \times 10^{-5}$	$5.475 \times 10^{-5}$	0.6937
400	0.5243	1069	0.05015	$8.951 \times 10^{-5}$	$3.261 \times 10^{-5}$	$6.219 \times 10^{-5}$	0.6948
450	0.4880	1081	0.05298	$1.004 \times 10^{-4}$	$3.415 \times 10^{-5}$	$6.997 \times 10^{-5}$	0.6965
500	0.4565	1093	0.05572	$1.117 \times 10^{-4}$	$3.563 \times 10^{-5}$	$7.806 \times 10^{-5}$	0.6986
600	0.4042	1115	0.06093	$1.352 \times 10^{-4}$	$3.846 \times 10^{-5}$	$9.515 \times 10^{-5}$	0.7037
700	0.3627	1135	0.06581	$1.598 \times 10^{-4}$	$4.111 \times 10^{-5}$	$1.133 \times 10^{-4}$	0.7092
800	0.3289	1153	0.07037	$1.855 \times 10^{-4}$	$4.362 \times 10^{-5}$	$1.326 \times 10^{-4}$	0.7149
900	0.3008	1169	0.07465	$2.122 \times 10^{-4}$	$4.600 \times 10^{-5}$	$1.529 \times 10^{-4}$	0.7206
1000	0.2772	1184	0.07868	$2.398 \times 10^{-4}$	$4.826 \times 10^{-5}$	$1.741 \times 10^{-4}$	0.7260
1500	0.1990	1234	0.09599	$3.908 \times 10^{-4}$	$5.817 \times 10^{-5}$	$2.922 \times 10^{-4}$	0.7478
2000	0.1553	1264	0.11113	$5.664 \times 10^{-4}$	$6.630 \times 10^{-5}$	$4.270 \times 10^{-4}$	0.7539

Note: For ideal gases, the properties  $c_p$ ,  $k$ ,  $\mu$ , and Pr are independent of pressure. The properties  $\rho$ ,  $\nu$ , and  $\alpha$  at a pressure  $P$  (in atm) other than 1 atm are determined by multiplying the values of  $\rho$  at the given temperature by  $P$  and by dividing  $\nu$  and  $\alpha$  by  $P$ .

Source: Data generated from the EES software developed by S. A. Klein and F. L. Alvarado. Original sources: Keenan, Chao, Keyes, Gas Tables, Wiley, 198; and Thermophysical Properties of Matter, Vol. 3: Thermal Conductivity, Y. S. Touloukian, P. E. Liley, S. C. Saxena, Vol. 11: Viscosity, Y. S. Touloukian, S. C. Saxena, and P. Hestermann, IFI/Plenum, NY, 1970, ISBN 0-306067020-8.



Performance Analysis and Simulation of Savonius Wind Turbine for Small-Scale Water Pumping System

---

Table B Standard Recommended Series of a Module (mm)

Choice 1	1.0 5.0	1.25 6.0	1.5 8.0	2.0 10	2.5 12	3.0 16	4.0 20
Choice 2	1.125 5.5	1.375 7	1.75 9	2.25 11	2.75 14	3.5 18	4.5
Choice 3	(3.25)	(3.75)	(6.5)				

Table C Standard diametral Pitches and Modules

**Table 12-3**

Standard Metric Modules

Metric Module (mm)	Equivalent $p_d$ ( $\text{in}^{-1}$ )
0.3	84.67
0.4	63.50
0.5	50.80
0.8	31.75
1	25.40
1.25	20.32
1.5	16.93
2	12.70
3	8.47
4	6.35
5	5.08
6	4.23
8	3.18
10	2.54
12	2.12
16	1.59
20	1.27
25	1.02

**Table 12-2**

Standard Diametral Pitches

Coarse ( $p_d < 20$ )	Fine ( $p_d \geq 20$ )
1	20
1.25	24
1.5	32
1.75	48
2	64
2.5	72
3	80
4	96
5	120
6	
8	
10	
12	
14	
16	
18	

Table D proportions of standard involute teeth(in terms of module m)

	<i>14.5° full depth system</i>	<i>20° full depth system</i>	<i>20° stub system</i>
Pressure angle	14.5°	20°	20°
Addendum	m	m	0.8 m
Dedendum	1.157 m	1.25 m	m
Clearance	0.157 m	0.25 m	0.2 m
Working depth	2 m	2 m	1.6 m
Whole depth	2.157 m	2.25 m	1.8 m
Tooth thickness	1.5708 m	1.5708 m	1.5708 m

Table E Values of the Lewis form factor (Y) for 20<sup>0</sup> full depth involute system

<b>z</b>	<b>Y</b>	<b>z</b>	<b>Y</b>	<b>z</b>	<b>Y</b>
15	0.289	27	0.348	55	0.415
16	0.295	28	0.352	60	0.421
17	0.302	29	0.355	65	0.425
18	0.308	30	0.358	70	0.429
19	0.314	32	0.364	75	0.433
20	0.320	33	0.367	80	0.436
21	0.326	35	0.373	90	0.442
22	0.330	37	0.380	100	0.446
23	0.333	39	0.386	150	0.458
24	0.337	40	0.389	200	0.463
25	0.340	45	0.399	300	0.471
26	0.344	50	0.408	Rack	0.484
(z = Number of teeth)					

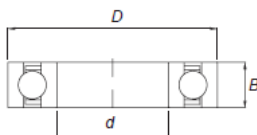
Table F Service factor for speed reduction gearboxes ( $C_s$ )

Working characteristics of Driving machine (Table 17.20)	Working characteristics of Driven machine (Table 17.21)		
	<i>Uniform</i>	<i>Moderate shock</i>	<i>Heavy shock</i>
Uniform	1.00	1.25	1.75
Light shock	1.25	1.50	2.00
Medium shock	1.5	1.75	2.25

Table G standard shaft diameter for key

Shaft diameter (mm) upto and including	Key cross-section		Shaft diameter (mm) upto and including	Key cross-section	
	Width (mm)	Thickness (mm)		Width (mm)	Thickness (mm)
6	2	2	85	25	14
8	3	3	95	28	16
10	4	4	110	32	18
12	5	5	130	36	20
17	6	6	150	40	22
22	8	7	170	45	25
30	10	8	200	50	28
38	12	8	230	56	32
44	14	9	260	63	32
50	16	10	290	70	36
58	18	11	330	80	40
65	20	12	380	90	45
75	22	14	440	100	50

Table H Inner and Outer diameter data for bearing



<i>d</i> (mm)	<i>D</i> (mm)	<i>B</i> (mm)	Basic dynamic load rating <i>C</i> (N)	Basic static load rating <i>C<sub>0</sub></i> (N)	Speed limit for grease lubrication (rpm)	Speed limit for oil lubrication (rpm)	Code
15	24	5	1570	800	28 000	34 000	61802
	32	8	5600	2850	22 000	28 000	16002
	32	9	5600	2850	22 000	28 000	6002
	35	11	7850	3750	19 000	24 000	6202
17	42	13	11 500	5 400	17 000	20 000	6302
	26	5	1690	930	24 000	30 000	61803
	35	8	6060	3250	19 000	24 000	16003
	35	10	6060	3250	19 000	24 000	6003
	40	12	9550	4750	17 000	20 000	6203
20	47	14	13 600	6550	16 000	19 000	6303
	62	17	23 000	10 800	12 000	15 000	6403
	32	7	2750	1500	19 000	24 000	61804
	42	8	6900	4050	17 000	20 000	16004
	42	12	9400	5000	17 000	20 000	6004
	47	14	12 800	6550	15 000	18 000	6204
	52	15	16 000	7800	13 000	16 000	6304
25	72	19	30 800	15 000	10 000	13 000	6404
	37	7	4400	2600	17 000	20 000	61805
	47	8	7600	4750	14 000	17 000	16005
	47	12	11 300	6550	15 000	18 000	6005
	52	15	14 050	7800	12 000	15 000	6205
30	62	17	22 600	11 600	11 000	14 000	6305
	80	21	36 000	19 300	9000	11 000	6405
	42	7	4500	2900	15 000	18 000	61806
	55	9	11 300	7350	12 000	15 000	16006
	55	13	13 400	8300	12 000	15 000	6006
	62	16	19 600	11 200	10 000	13 000	6206
30	72	19	28 200	16 000	9000	11 000	6306
	90	23	43 700	23 600	8500	10 000	6406

Table I Tolerances in microns on the adjacent pitch

Grade	<i>e</i> micron	Grade	<i>e</i> micron
1	0.80 + 0.06 $\phi$	7	11.0 + 0.90 $\phi$
2	1.25 + 0.10 $\phi$	8	16.00 + 1.25 $\phi$
3	2.00 + 0.16 $\phi$	9	22.00 + 1.80 $\phi$
4	3.20 + 0.25 $\phi$	10	32.00 + 2.5 $\phi$
5	5.00 + 0.40 $\phi$	11	45.00 + 3.55 $\phi$
6	8.00 + 0.63 $\phi$	12	63.00 + 5.00 $\phi$

Gears of grades 11 and 12 are manufactured by casting. Gears of grades 8 and 9 require rough and fine hobbing. Grade 6 is obtained by hobbing and rough grinding. Grade 4 requires shaving and finishing operations.

# Performance Analysis and Simulation of Savonius Wind Turbine for Small-Scale Water Pumping System

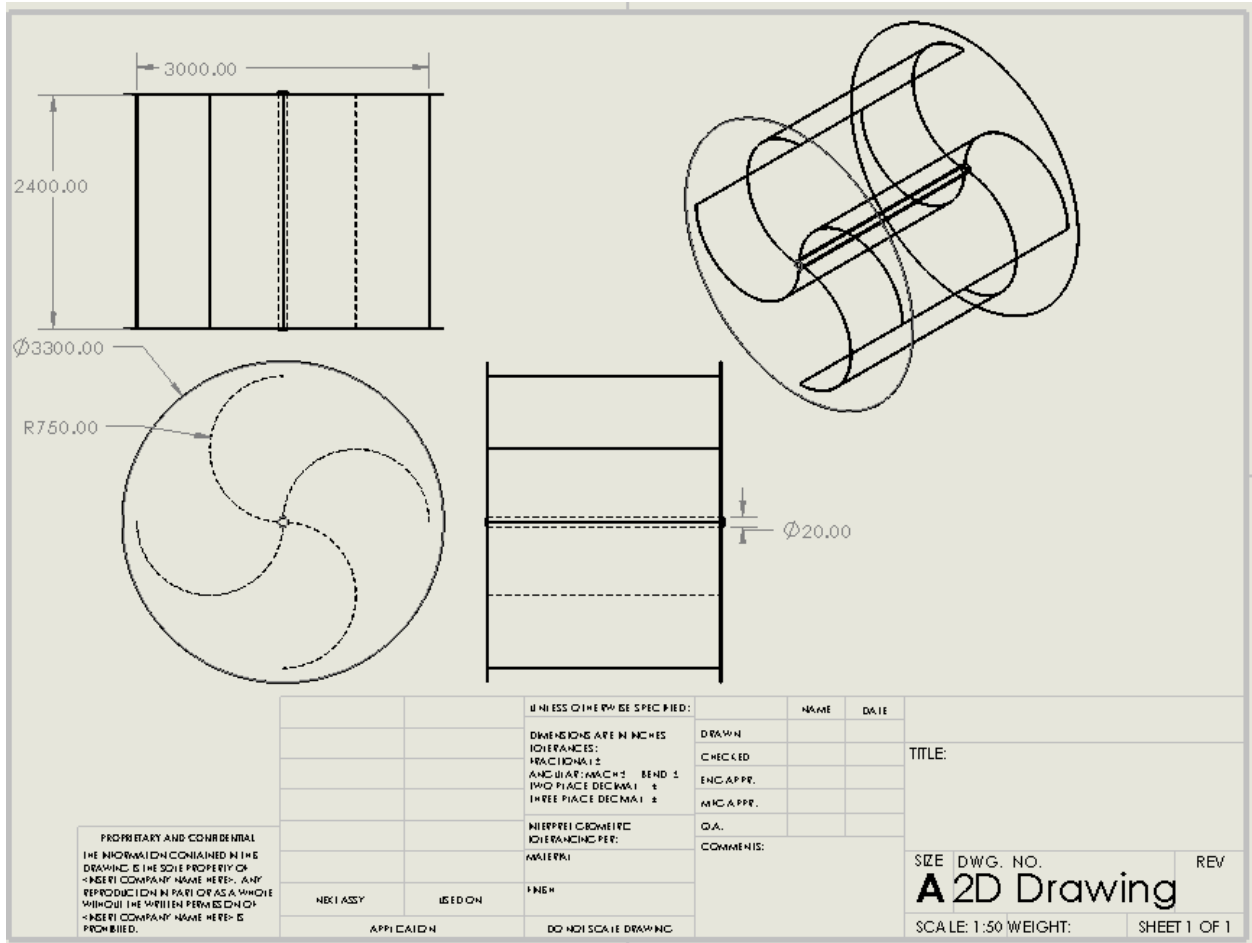


Fig The 2D geometry of the Savonius rotor



# JIMMA UNIVERSITY

ጅማ ዩኒቨርሲቲ

Ref No: FME/JIT/210/2013

ቁጥር

Date: 10/12/2013

ቀን

From: Faculty of Mechanical Engineering

Jimma institute of Technology

Jimma

To: National Metrological Agency

Addis Ababa

Sub: Request for data collection from Ethiopia Metrological Agency

As it is tried to emphasize on the subject, one of our students is in her 2nd year MSc study in Thermal Systems Engineering at Faculty of Mechanical Engineering, Jimma Institute of Technology, Jimma University. She would like to conduct her Research with the title Performance Analysis of Savonius wind turbine for water pumping system for Partial fulfillment of her MSc study. Therefore, she want to collect her data from your office.

The detail of the student and her research title is given in the table below.

Name of Student	ID No	Title of research
Abeba Negewo	RM/8575/11	Performance Analysis of Savonius wind turbine for water pumping system

Therefore, this is to kindly request your office cooperation to perform the aforementioned task. We would like to thank in advance for your kind cooperation.

Kind Regards,

Wendimu Fanta  
Transformation, AQA, Internship,  
& CBE Coordinator, Faculty of  
Mechanical Engineering



Tel: +251-471111457  
PBX: +251471111458-60

Fax: +25147111450  
+251471112040

P. O. Box: 378  
JIMMA, ETHIOPIA

mail: [ero@ju.edu.et](mailto:ero@ju.edu.et)  
website:  
<http://www.ju.edu.et>